Abstract

HI, infrared, CO, Hα and B-band observations of M51, the prototypical grand-design spiral galaxy, are used to study the consequences of star formation for the distribution of HI and dust. Using the new VLA map of 21-cm emission, our OVRO CO mosaic map, and an Hα image, we carry out new tests of the idea of Tilanus and Allen that the HI is largely a photodissociation product in star-forming regions. We confirm that the HI spiral arms are generally coincident with the HII region arms, and offset downstream from the CO arms. The radial distributions of total gas, Hα and HI surface density have a simple explanation in the dissociation picture. The distributions also demonstrate how the surface density of HI might be related to the star formation efficiency in molecule-rich galaxies. The large width of the HI regions along the arms compared to that of the giant HII regions can be understood in terms of a simple calculation of the expected size of an HI region associated with a typical giant HII region. The longer lifetime of the stars producing dissociating radiation *vs.* those producing ionizing radiation and the relatively long molecule formation timescale will also contribute to the greater width of the HI arms if stars are continuously forming on the arms. The lack of detailed coincidence of the HI and HII regions along the inner arms has a variety of possible explanations within the dissociation scenario.

We carry out two simple tests to probe the origins of the *IRAS* emission in M51. First, we find that the infrared excess (IRE) of M51 is 24, suggesting that a substantial fraction of the infrared emission arises from dust heated by photons which *do not* originate in massive star-forming regions. Second, radial cuts through the *IRAS* bands show that at 12, 25 and 60 μm, the arm-interarm contrast of the *IRAS* emission is substantially less than that of the Hα emission (convolved to matching resolutions), providing further evidence for the above explanation and for the existence of a broadly distributed dust component. Deconvolved *IRAS* maps have improved resolution but do not change this finding.

Subject headings: galaxies: interstellar matter – galaxies: individual (M51) – stars: formation – infrared: sources

I. Introduction

Great advances in our understanding of how spiral density waves organize atomic and molecular gas in galaxies and how they therefore relate to ongoing star formation have been made possible in the past few years with the advent of high-resolution centimeter- and millimeter-wave interferometers. M51 has been a popular target for such studies because of its proximity (distance 9.6 Mpc; Sandage and Tammann 1975), nearly face-on aspect, strong spiral structure, and molecule-rich ISM (about 90% of the ISM is molecular; Scoville and Young 1983). Observations of the ISM of this galaxy have been recently reviewed by Rand and Tilanus (1990).

In two previous papers (Vogel, Kulkarni, and Scoville 1988, hereafter VKS; Rand and Kulkarni 1990a, hereafter RK) we have presented mosaic maps of CO (1–0) emission from M51 at 8" resolution made with the Millimeter Interferometer of the Owens Valley Radio Observatory (OVRO). We detected molecular spiral arms which are well aligned with the dust lanes but offset upstream from the HII region arms (see Figure 1*a,b*), implying that the onset of massive star formation occurs several million years after the peak compression of the molecular gas. The spiral arms represent about one-third of the total emission measured with single dish instruments. The tangential and radial velocity shifts predicted by density wave theory as the gas is being compressed can be clearly seen where the arms cross the major and minor axes of the galaxy. Using Hα emission as a tracer of the massive star formation rate, we found that the star formation efficiency is higher on the arms than between the arms, implying that the density wave is triggering excess star formation from the compressed gas. This result has been confirmed in single-dish CO observations (Lord and Young 1990). The molecular arms contain well-organized structures which we termed Giant Molecular Associations (GMAs). The typical mass of a GMA is 3×10^7 $M_\odot$. GMAs are also found between the arms. The on-arm GMAs show a rough equality of virial and CO-flux based masses, while the interarm GMAs have virial masses several times their CO-flux based masses. The CO (1–0) spectra of the GMAs show that they typically consist of one to five velocity components. The GMAs may form through collisional agglomerations of pre-existing smaller clouds or by gravitational instabilities in the molecular gas (see Rand and Kulkarni 1990b). The interarm GMAs may owe their existence to a weak, secondary compression of the density wave.

VKS and RK examined how the density wave organizes the molecular gas and discussed the consequences for star formation from analysis of Hα images. In this paper, we further examine the "back reaction" of star formation on the ISM of M51 by considering, in conjunction with molecular data and an Hα image, the distribution of atomic gas and infrared emission from two new data sets: the VLA maps of 21-cm emission by Rots *et al.* (1990, hereafter RBHAC), and the *IRAS* (Infrared Astronomical Satellite) pointed observations of M51 (Rice *et al.* 1988).

Recently, evidence has been presented that in the molecule-rich galaxies M51 (Tilanus and Allen 1989, hereafter TA) and M83 (Allen, Atherton, and Tilanus 1986) HI is predominantly a product of dissociation of H_2 in star-forming regions. If the detected HI were distributed in the same way as all the gas we would expect to see the peak of the 21-cm emission along the dust lanes, where the highest compression of the gas is occurring. However, the observations show that in these galaxies HI is concentrated downstream from the dust lanes but coincident with the HII region arms. TA estimate that in M51 approximately 10% of the molecular gas is dissociated in star-forming regions. From their new VLA data, RBHAC produced maps at several resolutions ranging from 5" to 34". In this paper, we use primarily a map at 8" resolution. Compared to the WSRT map of TA, this map has higher angular resolution (8" x 8" *vs.* 12" x 18") and sensitivity. We use this map, along with our Hα and *B*-band images, CO data (see RK) and published single-dish CO data to carry out further quantitative tests of the dissociation scenario. In particular, we examine whether *a)* the radial distributions of total gas, Hα and HI, *b)* the small-scale structure of the HI emission and *c)* the detailed spatial relationship between the HI and HII regions can be explained in this picture. We find that the new VLA map provides much evidence in favor of the dissociation scenario.

Radiation from young stars not only ionizes HI and dissociates H_2 but also heats the interstellar dust. The infrared emission from dust allows yet another probe of the back reaction of star formation on the ISM. In the second part of this paper, we use the *IRAS* pointed observations of M51 to study the distribution and origins of the infrared emission. Recent work on the *IRAS* spectra of our Galaxy and other spirals (Cox and Mezger 1987; Lonsdale-Persson and Helou 1987; Helou 1986) has led to a picture for the dust emission in which the 12 μm emission is dominated by very small grains transiently heated by the interstellar radiation field (ISRF; there may also be a contribution from OH/IR stars), the 25 and 60 μm emission is from warm dust in star-forming regions but may also have a substantial contribution from generally distributed dust heated by the ISRF (or intermediate-mass young stars), and the 100 μm emission is dominated by relatively large grains heated by the ISRF. The very small grains are expected to be destroyed in star-forming regions (Puget, Léger, and Boulanger 1985), so little 12 μm emission is expected from such regions. Broadly distributed dust heated by the ISRF has come to be referred to as "cirrus" (Low *et al.* 1984). We use this term here to refer to both dust heated by the ISRF and by non-ionizing young stars.

We attempt to interpret the infrared emission of M51 in terms of these two components: dust in star-forming regions and cirrus. In particular, we carry out two tests designed to distinguish between infrared emission arising from massive star-forming regions, and emission from a cirrus component. We first calculate the "Infrared Excess" (IRE; Mezger 1978), a dimensionless quantity which provides a measure of the fraction of the infrared flux which arises from dust heated by photons which originate in massive star-forming regions. We then compare cuts

through the *IRAS* maps with cuts through Hα and *B*-band CCD images convolved to the *IRAS* resolutions to determine whether the infrared emission is distributed in the same way as the optical line emission from star-forming regions. If the infrared emission shows a reduced concentration to the spiral arms compared to the Hα emission, then one can conclude that a fraction of the infrared emission arises from generally distributed dust. We find that the results of both these tests indicate that a substantial fraction of the emission detected by *IRAS* is in fact in a cirrus component.

II. Hα Observations

Our Hα image was obtained at the 60 inch (1.5 m) telescope of the Palomar Observatory in June 1988, using the reimaging "Wide Field PFUEI" system. This same image was first shown in RK. However, the observations were only briefly described there. Observations were made with a 20 Å-wide Hα filter (redshifted to 500 km s^{-1}) and two adjacent 100 Å-wide continuum filters. The pixel size is 1.2". Registration and continuum subtraction were achieved through the use of a grid of stars. (EXPOSURE TIME? CHECK LOGS, REDUCTION NOTES).

A rough calibration was carried out by comparing our measured fluxes for nine HII regions in the inner disk to the published values of van der Hulst *et al.* (1988, hereafter HKCR). The scatter in this comparison is 20%, which is sufficiently low for our purposes. We corrected for extinction by assuming a mean value of $A_V = 2$ mag from HKCR. These authors found no significant dependence of A_V on galactocentric radius. Our resulting profile agrees very well with that of Lord and Young (1990), who used digitized versions of the photographic plates of Hodge and Kennicutt (1983). The Hα intensities may not be reliable for the region $R < 25$": the continuum images used for the continuum subtraction were saturated over parts of this region.

III. HI and Dissociation

In Figure 1*c,d* we show the VLA HI map of RBHAC overlaid on our CO map and Hα image. It is clear that compared to the CO distribution there is enhanced HI emission in the outer ($R \gtrsim 100$") arms, although the azimuthally averaged surface density of HI never contributes more than about 20% of the total gas surface density (Figure 2). Comparing with the OVRO CO map, we find a typical ratio of H_2 to HI column density in the inner arms of about 16. Therefore the new VLA map confirms the low HI/H_2 ratio on the arms, and the conclusion of TA that only a small fraction of the molecular gas is dissociated.

Table 1 gives typical arm and interarm surface densities for the inner disk. The Hα image was convolved to 13" resolution for the purpose of calculating these numbers to allow a comparison at matched resolutions. Surface densities of the

ionized gas were calculated assuming a temperature of 7000 K, a visual extinction of $A_V = 2$ mag (the typical values found by HKCR for the giant HII regions), a full-thickness of 250 pc for the gas layer, and a filling factor of $\phi = 0.1$. Because of scattering and reflection problems in the point-spread function of the reimaging camera used to obtain the Hα image (see Rand, Kulkarni, and Hester [1990] for a discussion of this point), the Hα arm-interarm surface density contrast may be somewhat reduced from its true value BY ???. These numbers demonstrate how little molecular gas is dissociated or ionized on the arms, and that the interarm gas is almost completely molecular.

a). Radial Distributions

The radial distributions of the total gas, Hα and HI surface density are shown in Figure 2. To estimate the total (H_2 and HI) gas surface density, we have used the FCRAO CO data at 45" resolution by Lord and Young (1990) and Scoville and Young (1983). To convert the CO emission to molecular column density, we assume the Galactic conversion factor of $\alpha = 3 \times 10^{20}$ mol cm^{-2} (K km s^{-1})$^{-1}$. All mass estimates in this paper include the Helium correction.

The total gas profile shows a roughly exponential fall-off with radius, while the Hα profile shows a similar fall-off, but with a pronounced enhancement at $R \approx 150$". The HI profile shows a central hole ($R \lesssim 30$"), a relatively flat inner disk ($30" \lesssim R \lesssim 100"$), a large enhancement in the outer disk peaking at $R \approx 150$", and finally a falloff at $R \gtrsim 175$". This profile can be understood in terms of the theory of Federman, Glassgold, and Kwan (1979), who consider the shielding of a molecular cloud to dissociating radiation by an outer envelope of HI. In this picture, the thickness of the dissociated envelope depends on the ratio of the dissociation and formation rates of H_2. This ratio has been shown by Hollenbach, Werner and Salpeter (1971) to depend on a power of G/n, where G is essentially the flux of dissociating radiation times the cross section in the Lyman bands of H_2, and n is the density of the gas.

Here we are considering the creation of dissociation regions in massive star-forming regions by energetic photons from young stellar associations. Since Hα traces the high-mass stars it should also trace the dissociating radiation. The flat HI profile in the inner disk and the large enhancement in HI around $R \approx 150$" can then be understood in terms of this simple balance between molecule formation and dissociation in star-forming regions. In the inner disk at $R \lesssim 100$", the Hα and total gas profiles show a similar falloff with radius, so that the balance between dissociation and formation changes little with radius and a constant column density of HI is produced. At $R \approx 150$", the "excess" of dissociating radiation in the outer arms relative to the gas density tips the scales in favor of dissociation, and thus more HI is produced. Beyond $R = 170$", the Hα enhancement ends, and the HI

returns to roughly its inner disk value. The radial distributions therefore support the dissociation picture.

If *i)* the HI emission is due to dissociated envelopes of *dense* clouds, as opposed to dissociated *diffuse* gas between the clouds, and *ii)* variations in the total gas surface density reflect variations in the number density of dense clouds, as opposed to variations in the gas density within the clouds, then the above explanation may not be valid. If all clouds have the same gas density, then the relative thickness of the dissociated envelopes would depend only on the relative intensity of the radiation field. then the observed local HI surface density would depend on the product of the local number density of clouds and the radiation field intensity, and the HI radial profile would be expected to drop off rather steeply with radius. However, while point *ii)* above may well be true, we show in the Appendix that the HI emission is almost certainly dominated by dissociated diffuse gas, and not by dissociated envelopes of dense clouds. Therefore, the dependence of the HI surface density on G and n discussed above is expected to pertain. This scenario only requires, then, that the total gas surface density profile reflects the density of the diffuse gas.

An interesting consequence of such an interpretation for the origin of the HI is that, since the Hα emission traces the star formation rate, the HI surface density is actually related to the star formation *efficiency* (the star formation rate per unit gas mass). The possibility of using HI as an indicator of star formation efficiency in molecule-rich galaxies such as M51 and M83 should be pursued further.

b). The Small-scale Structure

From the VLA HI map (Figures 1*c,d*) we note the following:

i) Over large sections of the inner ($R \lesssim 100$") arms (see Figure 1*c*) an offset can be seen between the centroids of the HI arms and CO arms, but the broad HI emission extends in many places upstream to the CO arms and often even *further* upstream into the pre-compression zone.

ii) The inner HI arms show a patchy structure and are broader than the Hα arms. The typical diameter (FWHM) of the bright HII regions in the inner arms is 5.5" or 250 pc, while the typical diameter of the HI arms is about 17" or 800 pc, although there is much variation in the latter quantity. When deconvolved from the 8" beam, the typical size becomes about 700 pc.

iii) While parts of the inner arms show a simple morphology in which HI envelopes exist around HII regions, there are many HI clouds which have very little Hα emission associated with them, as in M83 (Allen, Atherton, and Tilanus 1986). Figure 3 is a close-up view of an arm segment which shows the detailed spatial correspondence (or lack of it) between the CO, 21-cm, and Hα emission.

iv) There are a few HI clouds in the interarm regions, where there is also very little Hα emission. It should be pointed out that the total mass of HI in the VLA 8"-resolution map is 2×10^9 $M_\odot$, which is only 40% of the mass found in the single-dish observations of Appleton, Foster, and Davies (1986) and Rots (1980). In fact, RBHAC report that, in their lower resolution VLA observations, there is broadly distributed HI between the arms at the level of about 10^{20} cm^{-2} which has been missed in the 8" map. This interarm emission may not make up the entire flux missing from the 8" map, but the fact that the total flux in this map is well below the single-dish value indicates that some emission has been resolved out.

Figure 4 shows cuts across typical gaseous features on the NW arm: a giant HII region (No. 83 of Carranza, Crillon, and Monnet [1969]), an HI emission feature 30" south of this HII region from the VLA map at 13" resolution, and a cut across the CO (2–1) arm obtained by hand digitization of the contour map of Garcia-Burillo and Guélin (1990) at 12" resolution. The 13" version of the VLA data was used because of its better sensitivity to interarm emission relative to the 8" version. The CO (2–1) brightness temperatures were converted to surface densities using the observed CO (2–1)/ CO (1–0) ratio of 0.7, from Garcia-Burillo and Guélin, and assuming the above value of α. A visual extinction of $A_V = 3.3$ mag (the value measured for this HII region by HKCR) and the above value of the ionized gas temperature were used to convert Hα intensity to Emission Measure.

The surface density of the atomic and ionized components is quite low compared to the molecular component in this typical star-forming region. Assuming the same full-thickness of the gas layer as above, we find that the peak Emission Measure of 4000 pc cm^{-6} corresponds to a surface density of about 10 $(\phi/0.1)^{1/2}$ $M_\odot$ pc^{-2}, where ϕ is the filling factor of the ionized gas. Giant HII regions in nearby galaxies tend to have low filling factors, with perhaps 0.02 being a typical value (Kennicutt 1984). Hence, the peak ionized surface density is only a few $M_\odot$ pc^{-2}, while the peak atomic surface density is about 20 $M_\odot$ pc^{-2}. These are an order of magnitude less than the peak molecular surface density of about 200 $M_\odot$ pc^{-2}. Thus, the figure demonstrates that in typical star-forming regions only a small fraction of the molecular gas is dissociated or ionized.

We now explore whether these diverse observational results can be explained in the framework of the dissociation model.

i) The HI-CO Offset

First, the fact that the HI arms are, like the Hα arms, offset from the CO arms supports the idea that the HI is produced in star-forming regions. If the HI arms seen in the VLA map simply consisted of gas compressed by the density wave, then we would expect the HI emission generally coincident with the CO emission. This is not the case, although in some places the HI arms do overlap the CO arms,

sometimes even extending upstream of the CO emission. In the dissociation model, this latter fact would imply that a small fraction of the molecular gas is dissociated by *downstream* star formation *before* it reaches the zone of peak compression.

ii) The HI Arm Width

At the minimum, the width of the HI arm must equal the typical size of an HI region associated with a typical giant HII region. In the Appendix, we calculate the expected size of the HI regions along the inner arms of M51 using the observed Hα luminosity of a typical inner-arm giant HII region to estimate the ionizing photon rate. The effects of dust opacity are included in the calculation by using the HII region extinctions published by HKCR. The ambient ISM (largely molecular; see discussion in the Appendix) is considered to consist of dense and diffuse components, with a varying fraction in each. The dense clouds were chosen to have properties of a typical Galactic GMC.

Our simple model can reproduce HI regions with diameters of about 500 to 800 pc, in reasonable agreement with the observed sizes. We find that almost all of the HI surface density in the dissociation features is contributed by the diffuse medium rather than by the dissociated envelopes of dense clouds. The diffuse medium in the best models has a typical density of about 10 mol cm^{-3} and constitutes about 10–25% of the observed gas surface density, while the dense clouds have a volume filling factor of roughly 0.05, and make up the remainder of the surface density.

Two additional effects will increase the width of the HI arms relative to the Hα arms. First, since the hotter stars evolve more rapidly, the ionizing radiation from a stellar cluster will disappear faster than the dissociating radiation, to which B and A stars can contribute significantly. Thus, if young stellar clusters are continuously being formed at the "front" of the arms, then the zone over which dissociating stars are found will be broader than the zone over which ionizing stars are found. Some of the HI regions, then, may be due to dissociation by multiple clusters formed at different times on the arms.

The width of the zone due to this effect can be estimated as follows. From simple blackbody approximations and an assumed Initial Mass Function, we find that the stars that dominate the dissociating flux are late O and early B stars, which have main sequence lifetimes of $\tau_{MS} \approx 1 - 2 \times 10^7$ yr. (This result is somewhat sensitive to the slope of the upper end of the IMF. It is certainly valid form a Miller-Scalo IMF, but for a Salpeter IMF, all O and early B stars contribute about equally to the dissociating flux). The component of circular velocity perpendicular to the arms is approximately $(\Omega_{rot} - \Omega_P) R \sin i$, where Ω_{rot} is the rotational angular velocity, Ω_P is the pattern speed of the density wave, i is the pitch angle of the spiral arms and R is the galactocentric radius. Tully (1974b) determined a pattern

speed for the density wave in M51 (scaled to a distance of 9.6 Mpc) of 37 km s^{-1} kpc^{-1}, and measured i to be 18.5°. The rotation curve is essentially flat at v_{rot} = 210 km s^{-1} (Tully 1974a; Scoville and Young 1983). Therefore, at a distance from the nucleus of R = 3 kpc, the width perpendicular to the arms of the zone where dissociating stars should be found, assuming that they are all formed at about the same spiral phase, is 0.7 "τ_{MS} (Myr) $\approx 7 - 14$". This number is an upper limit since the orbits in a density wave compression bend to become more aligned with the spiral pattern compared to purely circular orbits, so that the "effective sin i" is reduced.

The second effect is that the atomic gas in the HI regions, once they have formed, will take a significant amount of time to recombine into molecules after the dissociating radiation disappears, leading to further downstream extension of the dissociation regions. The H_2 reformation timescale, $(Rn_H)^{-1}$, where R is the molecule formation constant (a value of 3 $\times 10^{-17}$ cm^{-3} s^{-1} was used in the models, see Appendix), and n_H is the total gas density (about 10 cm^{-3} in the best models), is roughly 10^8 yr. If the gas is clumped with filling factor ϕ, this timescale will be reduced by ϕ. For $\phi \sim 0.1$, the width perpendicular to the arms corresponding to the reformation timescale is $\sim$ 7".

The width of the HI arms is therefore likely due in part to these two effects. The width expected from these effects is larger near the Inner Lindblad Resonance of the wave and smaller near corotation. It seems, though, that the main reason for the HI arm width is the large size of the HI regions, as indicated by our models.

The molecule reformation timescale may be compared to the time between arm passages, $\pi(\Omega_{rot} - \Omega_P)^{-1}$, to see whether a steady state between dissociation and reformation can be maintained. With the above parameters, the time between arm passages is 5×10^7 yr at 2 kpc from the nucleus, and 2×10^8 yr at 4 kpc. Thus it is plausible that the dissociated gas can reform into molecules before the next arm passage such that a steady state is maintained, if the gas is moderately clumpy. The paucity of HI features between the arms in the 8" map may also be due to the rapid dilution of the on-arm features as they move off the arms by the expansion and shear of the underlying flow.

Finally, we note a perhaps surprising result from the calculation in the Appendix. We find from two independent methods of estimating the dust surface density that, in the inner disk, the dust-to-gas ratio (which is a necessary number for calculating the H_2 formation rate) is about equal to the Galactic value. This near equality of dust-to-gas ratios in M51 and the Galaxy may be a cause for concern given that the typical metallicity in the inner disk of M51 is three times the Solar value (Pagel and Edmunds 1981), so that one might expect a higher dust abundance.

iii) Poor Detailed Spatial Coincidence of HI and HII Regions

It remains to be explained why the detailed spatial coincidence of HII and HI regions is poor, particularly in the inner regions where the existence of the density wave has been established. One possibility, still within the above dissociation scenario, is that some of the HI clouds on the arms are simply regions of low total gas density compared to the typical on-arm density. In terms of the Federman, Glassgold, and Kwan (1979) model, for a given flux of radiation, the HI column density is high in these regions because the molecule formation timescale is relatively long. In other words, G/n is relatively high. However, a visual inspection of Figures 1*c* and 1*d* shows that HI regions not associated with Hα emission are sometimes associated with CO emission, and sometimes not, indicating that the HI is not necessarily found in regions of low total gas density.

We prefer the following effects as the more likely reasons for the lack of correlation. First, as mentioned above, the ionizing radiation from a stellar cluster disappears faster than the dissociating radiation because of the longer characteristic lifetime of the stars providing the dissociating radiation. Also, the molecule reformation timescale is much longer than the recombination timescale, so the 21-cm emission will persist well after the dissociating radiation disappears, whereas the ionized gas will quickly recombine once the ionizing radiation disappears. These effects would not only lead to a lack of correlation but would also explain why some HI regions extend preferentially downstream from the HII regions (Figure 1*d*). Another possible contributor could be the inevitable supernovae, which will clear out the immediate vicinity of the cluster, where the Hα emission is concentrated, much more effectively than the regions where the HI is found, much further away from the cluster center. The timescale for this clearing process may be comparable to the age of $\sim 10^7$ yr inferred by Brinks and Bajaja (1986) for the ~ 500 pc diameter HI holes they found in M31. Finally, if some clusters form without many OB stars, they may produce HI regions with little Hα emission.

iv) Interarm HI

The surface density of the smoothly distributed interarm component reported by RBHAC is about 10^{20} cm^{-2}. This component presumably consists of diffuse gas and dense cloud envelopes which are dissociated either by the ISRF or interarm star formation. The few interarm clouds compact enough to be seen in the 8"-resolution map do not have much associated Hα emission. They may be dissociation regions around stellar clusters with few OB stars.

IV. Infrared Properties

The aim of this analysis is to understand whether or not the infrared emission in M51 arises purely from star-forming regions. Figure 5 shows the *IRAS* maps of M51, while Table 2 lists some of the global properties of the infrared emission. T_W and T_C in Table 2 are the resulting temperatures in a two component fit to the *IRAS* data by Rice *et al.* (1988). T_C for M51 is $\lesssim 1\sigma$ above the mean value of all large optical galaxies modelled in this way by Rice *et al.* (1988).

Our first diagnostic is the dimensionless IRE, which is defined as the total *IRAS* flux, F_{IRAS}, (νf_ν summed over the four *IRAS* bands, although some authors use the 60 and 100 μm bands only) divided by the Lyman continuum flux. Mezger, Smith, and Churchwell (1974) calculate the infrared emission expected from an HII region for a given ionizing photon rate, and show how this photon rate can be estimated from the thermal flux density. The IRE is calculated as follows (Rice *et al.* 1990):

$$\mathrm{IRE} = 9.4\ (\mathrm{Hz}^{-1})\ \frac{F_{IRAS}(10^{-13}\mathrm{Wm}^{-2})}{S_{21}(\mathrm{mJy})} \qquad (1)$$

where S_{21} is the thermal continuum flux at 21 cm. The IRE is defined such that a value of unity means that all of the infrared emission can be explained as arising from dust heated by Lyα photons which were produced by absorption and degradation of the emergent Ly-continuum by the gas. An IRE greater than one implies that some of the infrared emission arises from dust heated *directly* by the Ly-continuum from H-ionizing stars and/or from dust heated by stars which provide little ionization.

The typical IRE found by Myers *et al.* (1986) for Galactic HII regions is 6. It is possible, however, that their balloon observations may have missed some of the shorter wavelength infrared emission since they employed only two detectors at 150 μm and 350 μm. However, Scoville and Good (1989), using all four *IRAS* bands to calculate the IR luminosity, found IREs ranging from 3 to 7 for four HII regions in the M17 and W51 regions. Furthermore, the *IRAS* study of M33 by Rice *et al.* (1990) showed that ten well-isolated HII regions with measurable IREs have values in the range 4–9 (the mean IRE over the whole galaxy is 14). Hence, these studies all indicate a typical IRE of 6 for HII regions. For a galaxy, an IRE well in excess of the value for Galactic HII regions indicates a substantial amount of infrared emission *not* due to dust heating by photons which originate in massive star-forming regions, but rather due to a "cirrus" component (see the Introduction).

In order to calculate the IRE, we need an estimate of the thermal continuum flux at 21 cm. Thermal-nonthermal flux separations have been carried out independently by Tilanus *et al.* (1988) and Klein, Wielebinski, and Beck (1984), with both studies finding a thermal flux at 21 cm of about 75 mJy. Thus the IRE of M51 is about 24, which is much higher than the typical value for Galactic HII

regions, indicating that a large fraction of the infrared luminosity arises from a cirrus component. One way to escape this conclusion is to invoke a much higher dust-to-gas ratio in M51, such that in the HII regions of M51, dust grains compete more effectively for ionizing photons than HI atoms relative to Galactic HII regions. However, we show in the Appendix that the dust-to-gas ratio is not significantly different from the Galactic value. Another possibility is that some fraction of the energetic photons escapes from the HII regions in M51 and is available to power a cirrus-like dust component and perhaps a diffuse, ionized medium. The thermal radio emission from the diffuse ionized gas may be too weak to detect, while the dust emission may be significant. However, to explain in this way the IRE of M51, which is fully four times the typical HII region IRE, almost all of the energetic photons responsible for the IR emission would have to escape from each HII region and be absorbed by generally distributed dust. Given that the typical visual extinction within the giant HII regions of M51 is about 0.5 mag (see the Appendix), the extinction at 1000 $\AA$ is about 2.2 mag, assuming the Galactic extinction curve. Although some of this extinction may be due to scattering and not absorption, it is unlikely that almost all of the photons around 1000 $\AA$ escape the HII region.

Our second test involves comparing the arm-interarm contrast in the *IRAS* maps with that in our Hα image convolved to the resolutions of the *IRAS* maps. The beam of the *IRAS* detectors is such that the resolution along the in-scan direction (position angle $\approx 45°$ for M51) is significantly better than that along the cross-scan direction. The in-scan resolution of the *IRAS* observations is sufficient for the measurement of an arm-interarm contrast at 12, 25 and 60 μm. The in-scan and cross-scan resolutions are listed in Table 3. If all of the infrared emission arises in star-forming regions, we would expect to see the same arm-interarm contrast in the infrared maps as in our Hα image.

Cuts in the in-scan direction of the original 12, 25 and 60 μm maps are presented in Figure 6 along with cuts through Hα and B-band images which have been convolved to the *IRAS* resolutions using the elongated *IRAS* beams. Ongoing star formation is traced by the Hα emission while the ISRF is best traced by the B-band light. The 100 μm cut is not shown because at the low resolution of the 100 μm data no spiral structure can be seen in either the map or the cut.

Features corresponding to the nuclear region and the outer NE and SW spiral arms can be seen in all of the cuts in Figure 6. It is clear that the arm-interarm contrasts in the cuts in all three *IRAS* bands are lower than those in the corresponding Hα cuts but higher than those in the B-band cuts. This result implies that in all three bands there is emission both from dust in star-forming regions and cirrus. For the warm dust (25 and 60 μm) this conclusion is not too surprising given the above discussion of the IRE. This conclusion is also understandable for the 12-μm emission if it is dominated by emission from very small grains which are

destroyed in star-forming regions. Note that the 12-μm arm-interarm contrast is slightly lower than that at 25 μm.

Deconvolved images of the *IRAS* pointed observations (see Neugebauer *et al.* 1984 for details of pointed observations) of M51 at all four *IRAS* bands were produced at the Infrared Processing and Analysis Center (IPAC) using a Richardson-Lucy deconvolution algorithm (Aumann, H. H., private communication). We examined maps at various stages of the deconvolution procedure and chose ones for the analysis below based on the level of spurious structure introduced in the blank regions around M51 by the deconvolution process. We judged that maps produced using more than 5 iterations at 12 and 25 μm and 20 iterations at 60 and 100 μm were possibly unreliable due to this rather subjective criterion. The deconvolved maps using the above numbers of iterations are shown in Figure 7, and the achieved resolutions are listed in Table 3. Cuts were made through these images as before, and are shown in Figure 8, along with Hα and B-band cuts at matched resolutions. Increases in the arm-interarm contrast can be clearly seen in the 12, 25 and 60 μm maps, but in the 100 μm map, the companion is only partially resolved and the outer arms remain unresolved. The 100 μm cut (not shown) shows no evidence for spiral structure.

The smoothness of the 100 μm map and cut is surprising when compared to Smith's (1982) map at 170 μm with 49" resolution (his Figure 2) made with the Kuiper Airborne Observatory. This map, at only slightly better resolution, shows clear spiral structure in the NE and SW. The longer wavelength of his observation should guarantee a smaller contribution to the emission from dust in star-forming regions, since this wavelength traces colder dust, thus reducing the expected contrast relative to that at 100 μm. The likely reason for this discrepancy is that the original 100 μm map had insufficient resolution to detect any spiral structure at all, even in the in-scan direction. Naturally, the deconvolution procedure would not bring out any spiral structure if there were none in the original data.

Figure 8 shows the same ordering of cuts by arm-interarm contrast as in Figure 6, and thus point to the same conclusion as that drawn from the original maps: there are at least two components to the infrared emission in the 12, 25 and 60 μm bands.

The deconvolution we have presented is by no means unique. For comparison, we show in Figure 9 a deconvolution of the 60 μm survey data by W. N. Weir (personal communication) using the MEMSYS software (based on the Maximum Entropy Method). This deconvolution method, unlike the Richardson-Lucy algorithm, does not assume that the point-spread function is constant over the field. The achieved resolution, although it almost certainly varies over the map, is obviously much better than that of Figure 7*c*, and a higher arm-interarm contrast in the outer arms can be seen. Unfortunately, a comparison of this map with the Hα

image would be perilous since the resolution varies over the map. It is therefore not clear how to perform the necessary convolution of the Hα image before the comparison. Compared to the pointed observations, the *IRAS* survey data unfortunately has a worse problem with striping in the in-scan direction, and a stripe can be seen running through the center of M51 in Figure 9 which confuses the interpretation.

We emphasize that our conclusions which are based on differences in arm-interarm contrast between the *IRAS* and Hα images do not depend on the reliability of the Richardson-Lucy deconvolution since the differences can be seen from the cuts through the *original IRAS* maps (Figure 6).

We can make a very rough estimate of the fractions of infrared emission which are associated with star-forming regions and ISRF-heated cirrus. Since the emissivity per dust grain of the cirrus component should be roughly proportional to the ISRF intensity, and since the cirrus arises from dust which is associated with the general gas distribution, the profile of cirrus emission should roughly resemble the product of the B-band profile and the profile of total gas surface density. The emission profile of dust in star-forming regions should roughly resemble the Hα profile. For the construction of the total gas profile the resolution of the FCRAO map is insufficient. We therefore use the new map of CO emission at 15" resolution from the Nobeyama 45-m and convolve it to the *IRAS* resolutions. Using this simple model and the profiles shown in Figure 6, we estimate that at 60 μm, 75% of the emission comes from the cirrus component, while 25% of the 25 μm emission and 75% of the 12 μm emission is due to cirrus. For M33, by way of comparison, a more careful decomposition by Rice *et al.* (1990) showed that cirrus accounts for 50% of the 12 and 60 μm emission, and 10% of the 25 μm emission. For both these galaxies then, the 25 μm band contains the highest fraction of emission from star-forming regions.

The results from these two tests imply that a direct interpretation of the *IRAS* luminosity of M51, either the total *IRAS* luminosity or L_{FIR} alone, in terms of a star formation rate, would be spurious. The same conclusion has been reached in studies of many other nearby spirals, where the IREs range from 13 to 24 (M33 [Rice *et al.* 1990]; M101 [Beichman *et al.* 1987]; and NGC 4565, NGC 891 and NGC 5907 [Wainscoat, de Jong, and Wesselius 1987]). Furthermore, studies of M31 (Walterbos and Schwering 1987) and the Galaxy (Bloemen, Deul, and Thaddeus 1990) have shown that most of the FIR emission arises from cirrus in these galaxies. Finally, Bothun, Lonsdale, and Rice (1989) found for most spiral galaxies in an optically selected sample – using f_{60}/f_{100} as a diagnostic of dust heating sources along with a simple dust-heating model – that dust in star-forming regions and cirrus are both important contributors to the total FIR luminosity.

The position of M51 in the color-color diagram of Helou (1986) confirms the above conclusion. In his Figure 2, M51 lies below the line where half of the infrared

emission derives from star-forming regions, implying that the cirrus contributes the majority of the emission.

Throughout this analysis, we have used the term "cirrus" to refer to emission from dust outside of regions of high-mass star formation. It should be noted, however, that Cox, Krügel, and Mezger (1986) conclude that non-ionizing young B and A stars could heat dust in star-forming regions to 30-40 K and provide some of the emission detected by *IRAS* in the Galaxy. It has been suggested for our Galaxy (see Scoville and Sanders 1988), although there is no direct evidence for M51, that B and A star formation is more uniformly distributed than O star formation. If this is the case in M51, then such an infrared emission component from regions of intermediate-mass star formation may have a spatial distribution more like the cirrus component and thus be observationally indistinguishable from cirrus based on the spatial distribution of far infrared (FIR) emission alone. It is therefore worth keeping in mind that radiation from "generally distributed dust" may have more than one origin. However, regardless of the nature of the cirrus, our tests have shown that the infrared emission cannot be accounted for by high-mass star formation alone.

An important consequence of the main conclusion of this section is that infrared emission cannot be used to independently test the hypothesis of density wave triggering of star formation unless the component of emission from star-forming regions can be effectively isolated, both spatially and spectrally. One should keep in mind that the arms which have been resolved or partially resolved by *IRAS* are beyond the radius of corotation of the density wave and are probably tidal arms generated by the passage of the companion (Tully 1974a; Elmegreen, Elmegreen, and Seiden 1989). Therefore, even the deconvolved *IRAS* images do not begin to resolve the density wave arms and hence cannot be used to test density wave triggering of star formation.

V. Conclusions

We have used VLA HI data and *IRAS* maps of M51 in an attempt to further understand the consequences of star formation in this molecule-rich galaxy with a strong density wave. From the HI map, we find compelling evidence which favors the idea that the HI is almost entirely a product of dissociation of H_2 in star-forming regions. The radial distribution of HI as well as the characteristic size of the emission features along the arms have simple explanations in the dissociation scenario. The lack of detailed correlation between HI and HII regions has a variety of possible causes. HI between the arms may be dissociated by the ISRF or by interarm star formation. There are indications that the gas-to-dust ratio is about equal to the Galactic value.

The IRE and the reduced arm-interarm contrast of the *IRAS* maps compared to the Hα image both indicate that a substantial fraction of the infrared emission

detected by *IRAS* does not arise in star-forming regions, but rather from dust associated with generally distributed gas ("cirrus"). The same conclusion has now been drawn for several nearby galaxies. An important implication of this result is that it will be difficult to interpret the FIR emission from M51 in terms of recent star formation, and thus to use FIR emission to check the hypothesis of density wave triggering of star formation. Regardless of whether a reliable separation of emission components can be done, the resolution of the *IRAS* maps is insufficient to resolve the inner, density-wave spiral arms.

Acknowledgements

We are deeply indebted to A. Rots for providing us with the VLA map of HI emission. We thank N. Nakai for allowing us to use the Nobeyama 45-m CO map in the discussion of the *IRAS* emission. We are grateful to N. Z. Scoville and E. S. Phinney for helpful comments. We thank W. N. Weir for his deconvolution of the 60 μm *IRAS* image, and we acknowledge the Maxent90 Image Reconstruction Contest and the Laboratory for Space Research in Groningen, the Netherlands, for permission to use this image. This work was partially supported by *IRAS* grant NAG 5-1164. The OVRO Millimeter Interferometer is supported by NSF grant AST 97-14405.

Appendix

We show here through a simplified radiative analysis that the large observed sizes of the discrete HI regions along the inner arms can be understood if they owe their existence to photo-dissociation of ambient H_2 by the OB associations (as indicated by the giant HII regions) along the arms. These HI regions have FWHM diameters of about 700 pc (when deconvolved from the 8" beam) and peak surface densities of about 20 $M_\odot$ pc^{-2} (see Figure 3).

A typical giant HII region has an extinction-corrected Hα luminosity of 5×10^{39} erg s^{-1} (HKCR), which corresponds to about 3.5×10^{51} ionizing photons per second, or the equivalent of 70 O5 stars (Kennicutt, Edgar, and Hodge 1989). We assume that all photons shortward of 13.6 eV are absorbed by H atoms, while photons with energies between 11.2 and 13.6 eV are available to dissociate H_2 molecules. Using simple blackbody approximations and a Salpeter Initial Mass Function, we estimate that the photon rate in the above energy range for a stellar cluster is about 50% of the ionizing photon rate. We use this ratio for the HI regions of M51.

Dissociation of H_2 occurs by excitation through photon absorption followed by a decay to the ground level with vibrational quantum number $v \geq 14$. Only about 23% of such absorptions lead to a dissociation (Dalgarno and Stevens 1970). We calculate the dissociation rate by the method of de Jong, Dalgarno, and Boland (1980), who consider only photon absorption in the Lyman band, and approximate that all 60 Lyman bands have an identical oscillator strength. The dissociation rate is given by their equation (A1). For the line opacity, we assume the regime in which photon absorption in the Lorentz wings of the lines dominates. De Jong, Dalgarno, and Boland estimate that this regime pertains for 10^{16} $cm^{-2} \lesssim N_{H_2} \lesssim 10^{22}$ cm^{-2}. The line opacity is then given by equation (A4) of de Jong, Dalgarno, and Boland, and is proportional to $N_{H_2}^{-1/2}$, where N_{H_2} is the molecular column density between the association center and the radius of interest. The dissociation rate at any radius from the center of the cluster is therefore

$$R_D = 2 \times 10^{-5} \frac{I}{I_H} e^{-2.5\,A_V} N_{H_2}^{-1/2} n(H_2) \qquad \text{(A1)}$$

where $\frac{I}{I_H}$ is the intensity of the radiation field in units of the Habing (1968) ISRF (2×10^{-8} photons cm^{-2} s^{-1} Hz^{-1} at 1000 Å), $n(H_2)$ is the number density of molecules, and A_V is the visual extinction between the association center and the radius of interest. The radiation field intensity, I, is readily calculated from the dissociating photon flux, geometrically diluted for the radius of interest.

The molecule formation rate at any radius is given by

$$R_F = R n_H n(HI) \qquad \text{(A2)}$$

where n_H is the total density of H and n(HI) is the density of atomic H. R is the H_2 formation constant (Spitzer 1978, p. 123), which is proportional to the projected area of dust grains per H nucleus, so that it must be scaled from the Galactic value of $R_{Gal} \approx 3.0 \times 10^{-17}$ cm^3 s^{-1} by the estimated dust-to-gas ratio contrast between M51 and our Galaxy (assuming similar grain properties). So equation (A2) becomes

$$R_F = R_{Gal} \frac{D_{M51}}{D_{Gal}} n_H n(\mathrm{HI}) \qquad \text{(A3)}$$

where D_{M51} and D_{Gal} are the dust-to-gas ratios in M51 and the Galaxy.

By balancing molecule formations with dissociations, one can solve for the atomic fraction at any distance from the source of dissociating radiation. If we define $f(r)$ to be the fraction of H atoms in molecular form at radius r from the association, then we obtain the following equation to be solved numerically for $f(r)$:

$$(1/f(r) - 1)\,(1/r \int_0^r f(r')\,dr') = 4.3 \times 10^6 \frac{D_{Gal}}{D_{M51}} \frac{I_{r_{HII}}}{I_H} e^{-2.5\,A'_V}\, r^{-5/2}\, n_H^{-3/2} \qquad \text{(A4)}$$

where $I_{r_{HII}}$ is the radiation field intensity at the radius of the HII region, taking into account extinction within the HII region, and A'_V is the extinction between the HII region and r.

The extinction in the HI and HII regions can be estimated from HKCR. From a comparison of the extinction at Hβ and the Hα-Hβ color excess with the models of Caplan and Deharveng (1986) for 11 giant HII regions, they deduce that only about 0.5 mag of the typical 1.8 mag of visual extinction could arise from within the HII regions, and that the remaining extinction occurs in foreground dust. We therefore assume that $A_V = 0.5$ mag over the $\sim$ 125 pc radius of the giant HII regions. At 1000 $\AA$ then, $\frac{I_{r_{HII}}}{I_H} \approx 25$ for our OB association.

The dust-to-gas ratio in the inner galaxy can simply be estimated from the typical visual extinction towards the HII regions of about 1.8 mag and the typical gas surface density along the HII region arms. The latter is estimated from the CO (2–1) map of Garcia-Burillo and Guélin (1990) to be about 140 M$_\odot$ pc $^{-2}$ at 3 kpc from the nucleus (assuming the value of α in the text). This extinction represents the contribution from the HII region and the dust layer above it. There should therefore be an additional 1.3 mag of extinction from the dust associated with the gas layer on the far side of the plane, leading to a total extinction of 3.1 mag in a gas column. Assuming the gas and dust are coextensive, these numbers imply a column density of 3×10^{21} cm^{-2} per magnitude of visual extinction, compared to the Galactic value of 2×10^{21} cm^{-2} (Spitzer 1978, p. 156, 161). The inferred dust-to-gas ratio is thus about equal to the Galactic value. A check on this number can be obtained from Smith's (1982) estimate of the dust mass surface density in the inner disk of M51 (Smith's "Bar" region) of 0.64 M$_\odot$ pc^{-2}. The dust-to-gas

mass ratio calculated in this way is thus 0.005, again about equal to the Galactic value. We also use this result to calculate the extinction per unit column density in the ISM outside of the HII region for use in equation (A4).

We must specify an "initial" state of the ISM (before it is modified by on-arm star formation) of M51. We assume that the ISM consists of dense and diffuse components. In contrast to our Galaxy, M51 should have a diffuse medium which is predominantly molecular as opposed to atomic (except possibly near star-forming regions). In the interarms, the HI surface density is ~ 1 $M_\odot$ pc^{-2} (RBHAC) while the H_2 surface density inferred from the map of Garcia-Burillo and Guélin is ~ 50 $M_\odot$ pc^{-2}. Hence, if the diffuse medium has any appreciable surface density at all relative to the cloudy medium, it should be largely molecular, with the atomic component contributing at most about 1 $M_\odot$ pc^{-2}. We therefore assume as an initial condition that the ISM outside of the HII region consists of two components: a uniformly distributed population of homogeneous dense clouds all with properties of a canonical Galactic GMC ($M = 4 \times 10^5$ $M_\odot$, $D = 40$ pc), and a uniformly distributed diffuse molecular medium between the dense clouds. The total molecular surface density in the region where the HI emission features and HII regions are found is constrained to be 140 $M_\odot$ pc^{-2}, as estimated from the map of Garcia-Burillo and Guélin. The full-thickness of the gaseous layer is initially taken to be 150 pc. Finally, we assume that there is no gas in atomic form within the HII region.

Our method is to assume fractions of the total surface density which are in dense clouds and diffuse gas, and calculate first the atomic fraction in the diffuse gas as a function of the distance from the cluster center. We call the distance at which the atomic fraction drops to 0.5 the "radius"of the HI region. For this calculation we need to know the volume filling factor of the dense clouds. This we calculate from the areal filling factor (equal to the assumed surface density of dense clouds divided by the observed total molecular surface density) and the assumed full-thickness of the gas layer. For any radiation field intensity of interest, the dense clouds will be completely opaque to the incident radiation and can be treated as opaque disks in the calculation for the diffuse component. From the volume filling factor and the assumed dense cloud diameter, we can calculate the attenuation per unit path length of the emergent flux from the cluster due to the dense clouds. We now have sufficient information to calculate the atomic fraction in the diffuse gas as a function of radius from the cluster center.

We then calculate the thickness of the dissociated envelopes of the dense clouds as a function of distance from the cluster, taking into account the attenuation in the diffuse molecular gas between the cloud and the cluster. We use a plane-parallel geometry for the cloud surfaces. The "thickness" is defined as the depth at which the atomic fraction drops to 0.5. Finally, we calculate the total HI surface

density as a function of distance from the cluster, approximating that the HI surface density per dense cloud will equal the volume density times the envelope thickness.

We first show that the dominant contributor to the HI surface density in a dissociation feature is the diffuse, not the dense, component. If *all* the gas is in canonical dense clouds, then we calculate that a dense cloud at the edge of the HII region (125 pc from the cluster) will have a dissociated envelope with a thickness of 0.3 pc. The corresponding surface density for the entire cloud system (for which the areal filling factor will be about 0.2) is only 1 $M_\odot$ pc^{-2}, whereas the HI features have typical surface densities of 10–20 $M_\odot$ pc^{-2} (see Table 1 and Figure 3). For an alternative estimate of the envelope thickness, we use the calculations of Federman, Glassgold, and Kwan (1979). Using their equation (10) and our parameters at 125 pc from the cluster, we find an envelope thickness of 0.7 pc. Hence, the negligible contribution from the dense clouds to the surface density is confirmed.

Figure 10 shows surface density profiles for various dense-diffuse fractions. To reproduce the observed HI region radius of 350 pc, the majority of the gas must be in the dense component. For diffuse fractions lower than shown in Figure 10, the modelled regions become too extended with surface densities too low, relative to observed regions. The necessary fraction in the diffuse component can be doubled by assuming that the gas layer has a full-thickness of 300 pc (Figure 10).

Our results, therefore, depend on the rather uncertain gas layer thickness and dense-diffuse fraction. We can, however, approximately reproduce an observed HI region with reasonable parameters. The sizes are somewhat underestimated for some cases. However, in the text we describe additional effects which may contribute to the large observed sizes of the dissociation features.

Table 1. Typical Arm and Interarm Gas Surface Densities

Component	$\Sigma_{\rm arm}$ ($M_\odot$ pc^{-2})	$\Sigma_{\rm interarm}$ ($M_\odot$ pc^{-2})
Molecular Gas	180	45
Atomic Gas	10	1
Ionized Gas	2	1

Table 2. Infrared Properties of M51

		Reference
$f_\nu(12\ \mu m)$	11 ± 5 Jy	Rice *et al.* 1988
$f_\nu(25\ \mu m)$	17 ± 6 Jy	"
$f_\nu(60\ \mu m)$	109 ± 4 Jy	"
$f_\nu(100\ \mu m)$	292 ± 7 Jy	"
$f_\nu(170\ \mu m)$	393 Jy	Smith 1982
L_{FIR} (40 μm–120 μm)	$1.9 \times 10^{10}\ L_\odot$	Rice *et al.* 1988
L_{FIR}/L_B	0.7	"
L_{IRAS} (5 μm–1 mm)	$5.0 \times 10^{10}\ L_\odot$	"
Infrared Excess (IRE)	24	This work
T_W	209.4 K	Rice *et al.* 1988
T_C	33.4 K	Rice *et al.* 1988

Table 3. Original and Deconvolved *IRAS* Map Resolutions

Band	Original Resolution	Deconvolved Resolution
	In-Scan/Cross-Scan FWHM	In-Scan/Cross-Scan FWHM
12 μm	45"/271"	30"/78"
25 μm	43"/271"	32"/81"
60 μm	83"/278"	33"/56"
100 μm	170"/290"	59"/69"

References

Allen, R. J., Atherton, P. D., and Tilanus, R. P. J. 1986, *Nature*, **319**, 296.

Appleton, P. N., Foster, P. A., and Davies, R. D. 1986, *M. N. R. A. S.*, **221**, 393.

Beichman, C., Boulanger, F., Rice, W., and Lonsdale Persson, C. J. 1987, in *Star Formation in Galaxies*, ed. C. J. Lonsdale Persson (NASA: CP 2466), p. 297.

Bloemen, H., Deul, E. R., and Thaddeus, P. 1990, preprint.

Bothun, G. D., Lonsdale, C. J., and Rice, W. 1989, *Ap. J.*, **341**, 129.

Brinks, E. and Bajaja, E. 1986, *Astr. Ap.*, **169**, 14.

Caplan, J. and Deharveng, L. 1986, *Astr. Ap.*, **155**, 297.

Carranza, G., Crillon, R., and Monnet, G. 1969, *Astr. Ap.*, **1**, 479.

Cox, P., Krügel, E., and Mezger, P. G. 1986, *Astr. Ap.*, **155**, 380.

Cox, P. and Mezger, P. G. 1987, in *Star Formation in Galaxies*, ed. C. J. Lonsdale Persson (NASA: CP 2466), p. 23.

Dalgarno, A., and Stevens, T. L. 1970, *Ap. J. (Letters)*, **160**, L107.

de Jong, T., Dalgarno, A., and Boland, W. 1980, *Astr. Ap.*, **91**, 68.

Elmegreen, B. G., Elmegreen, D. M. and Seiden, P. E. 1989, *Ap. J.*, **343**, 602.

Federman, S. R., Glassgold, A. E., and Kwan, J. 1979, *Ap. J.*, **227**, 466.

Garcia-Burillo, S., and Guélin, M. 1990, preprint.

Habing, H. J. 1968;Bull. Astr. Inst. Netherlands;19;421

Helou, G. 1986, *Ap. J. (Letters)*, **311**, L33.

Hodge, P. W. and Kennicutt, R. C. 1983, *A. J.*, **88**, 296.

Hollenbach, D., Werner, M. W., and Salpeter, E. E. 1971, *Ap. J.*, **163**, 155.

Kennicutt, R. C. 1984, *Ap. J.*, **287**, 116.

Kennicutt, R. C., Edger, B. K., and Hodge, P. W. 1989, *Ap. J.*, **339**, 761.

Klein, U., Wielebinski, R., and Beck, R. 1984, *Astr. Ap.*, **135**, 213.

Lonsdale-Persson, C. J. and Helou, G. 1987, in *Star Formation in Galaxies*, ed. C. J. Lonsdale Persson (NASA: CP 2466), p. 23.

Lord, S. D., and Young, J. S. 1990, *Ap. J.*, **356**, 135.

Low, F. J. *et al.* 1984, *Ap. J. (Letters)*, **278**, L19.

Mezger, P. G. 1978, *Astr. Ap.*, **70**, 565.

Mezger, P. G., Smith, L. F., and Churchwell, E. 1974, *Astr. Ap.*, **32**, 269.

Myers, P. C., Dame, T. M., Thaddeus, P., Cohen, R. S., Silverberg, R. F., Dwek, E., and Hauser, M. G. 1986, *Ap. J.*, **301**, 398.

Neugebauer, G. *et al.* 1984, *Ap. J. (Letters)*, **278**, L1.

Pagel, B. E. J., and Edmunds, M. G. 1981, *Ann. Rev. Astr. Ap.*, **19**, 77.

Puget, J. L., Léger, A., and Boulanger, F. 1985, *Astr. Ap.*, **142**, L19.

Rand, R. J., and Kulkarni, S. R. 1990a, *Ap. J. (Letters)*, **349**, L43 (RK).

Rand, R. J., and Kulkarni, S. R. 1990b, in preparation.

Rand, R. J., Kulkarni, S. R., and Hester, J. J. 1990, *Ap. J. (Letters)*, **352**, L1.

Rand, R. J. and Tilanus, R. P. J. 1990, in *The Interstellar Medium in Galaxies*, eds. H. A. Thronson and J. M. Shull (Dordrecht:Kluwer), p. 525.

Rice, W., Boulanger, F., Viallefond, F., Soifer, B. T., and Freedman, W. L. 1990, *Ap. J.*, **358**, 418.

Rice, W., Lonsdale, C. J., Soifer, B. T., Neugebauer, G., Kopan, E. L., Lloyd, L. A., De Jong, T., and Habing, H. J. 1988, *Ap. J. Suppl.*, **68**, 91.

Rots, A. H. 1980, *Ap. J. Suppl.*, **41**, 189.

Rots, A. H., Bosma, A., van der Hulst, J. M., Athanassoula, E., and Crane, P. C. 1990, *A. J.*, **100**, 387 (RBHAC).

Sandage, A., and Tammann, G. A. 1975, *Ap. J.*, **196**, 313.

Scoville, N. Z., and Good, J. C. 1989, *Ap. J.*, **339**, 149.

Scoville, N. Z., and Sanders, D. B. 1987, in *Interstellar Processes*, ed. D. Hollenbach and A. Thronson (Dordrecht: Reidel), p. 21.

Scoville, N. Z., and Young, J. S. 1983, *Ap. J.*, **265**, 148.

Smith, J. 1982, *Ap. J.*, **261**, 463.

Spitzer, L. J. 1978, *Physical Processes in the Interstellar Medium* (New York: Wiley).

Tilanus, R. P. J., and Allen, R. J. 1989, *Ap. J. (Letters)*, **339**, L57 (TA).

Tilanus, R. P. J., Allen, R. J., van der Hulst, J. M., Crane, P. C., and Kennicutt, R. C. 1988, *Ap. J.*, **330**, 667.

Tully, R. B. 1974a, *Ap. J. Suppl.*, **27**, 437.

Tully, R. B. 1974b, *Ap. J. Suppl.*, **27**, 449.

van der Hulst, J. M., Kennicutt, R. C., Crane, P. C., and Rots, A. H. 1980, *Astr. Ap.*, **195**, 38 (HKCR).

Vogel, S. N., Kulkarni, S. R., and Scoville, N. Z. 1988, *Nature*, **334**, 402 (VKS).

Wainscoat, R. J., de Jong, T., and Wesselius, P. R. 1987, *Astr. Ap.*, **181**, 225.

Walterbos, R. A. M. and Schwering, P. B. W. 1987, *Astr. Ap.*, **180**, 27.

Figure Captions

FIG. 1. Shown in the top left panel are contours of CO emission from the OVRO mosaic overlaid on a red CCD image. The contour levels are as stated in RK. The top right panel shows CO contours overlaid on an Hα CCD image. The bottom left panel shows contours of CO overlaid on a grey-scale representation of the VLA 21-cm map. The bottom right panel shows contours of 21-cm emission on the Hα image. The contour levels are 1, 1.5, 2, and 4 times 8.4×10^{20} cm^{-2} in the bottom right panel.

FIG. 2. The radial distributions of total gas (H_2 plus HI) surface density, Hα emission, and HI surface density. The radial profiles of Lord and Young (1990, for $R < 150$") and Scoville and Young (1983, for $R > 150$") have been converted to surface density units assuming $\alpha = 3 \times 10^{20}$ mol cm^{-2} (K km s^{-1})$^{-1}$. The Hα intensities have been corrected for $A_V = 2$ mag of extinction (see van der Hulst *et al.* (1988).

FIG. 3. A close-up of a spiral arm segment south of the nucleus showing the small scale relationship between HI, Hα and CO emission. The solid contours are HI emission. The levels are 1, 2, 3, 4, and 5 times 8.4×10^{20} cm^{-2}. The dashed contours are CO emission from the OVRO mosaic. The grey-scale represents Hα emission. The flow direction is indicated. The area labelled "A" is an example of a region where an HI peak coincides with an HII region. The areas labelled "B" are examples of HI peaks *between* HII regions.

FIG. 4. Cuts in surface density through typical on-arm molecular, atomic and ionized gas features along the NW arm: (*solid line*) a cut across the CO (2–1) arm of Garcia-Burillo and Guélin (1990; see text for the conversion from CO (2–1) flux to surface density), (*dashed line*) a cut through a prominent HI emission feature on the NW arm, and (*dot-dashed line*) a cut through a typical giant HII region on the same arm (see text for the conversion of Hα flux to surface density). The peak EM of the HII region roughly corresponds to 10 $(\phi/0.1)^{-1/2}$ M$_\odot$ pc^{-2}, where ϕ is the filling factor of the ionized gas.

FIG. 5. The original maps of *IRAS* emission in M51: *a)* 12μm, *b)* 25μm, *c)* 60μm, and *d)* 100μm. The unit contour interval is the estimated noise in the map.

FIG. 6. Cuts through the original *IRAS* maps and Hα and *B*-band CCD images along the *IRAS* in-scan direction from NE to SW.

FIG. 7. The deconvolved maps of *IRAS* emission in M51: *a)* 12μm, *b)* 25μm, *c)* 60μm, and *d)* 100μm. The unit contour interval is the estimated noise in the map.

FIG. 8. Cuts through the deconvolved *IRAS* maps and Hα and B-band CCD images along the *IRAS* in-scan direction from NE to SW.

FIG 9. Deconvolution of the *IRAS* 60μm survey data on M51 by W. N. Weir using the MEMSYS package. The contour levels are 5, 10, 15, 20, 25, 30, 35, 40, 50, 60, 70, 80, and 90 percent of the peak.

FIG 10. Profiles of HI surface density for five model dissociation regions with varying dense cloud-diffuse gas fractions and gas disk full-thicknesses: *(solid line)* all diffuse gas, full-thickness 150 pc, *(dotted line)* 50% diffuse gas, full-thickness 150 pc, *(short-dashed line)* 25% diffuse gas, full-thickness 150 pc, *(long-dashed line)* 13% diffuse gas, full-thickness 150 pc, and *(dot-dashed line)* 25% diffuse gas, full-thickness 300 pc.

Fig 1

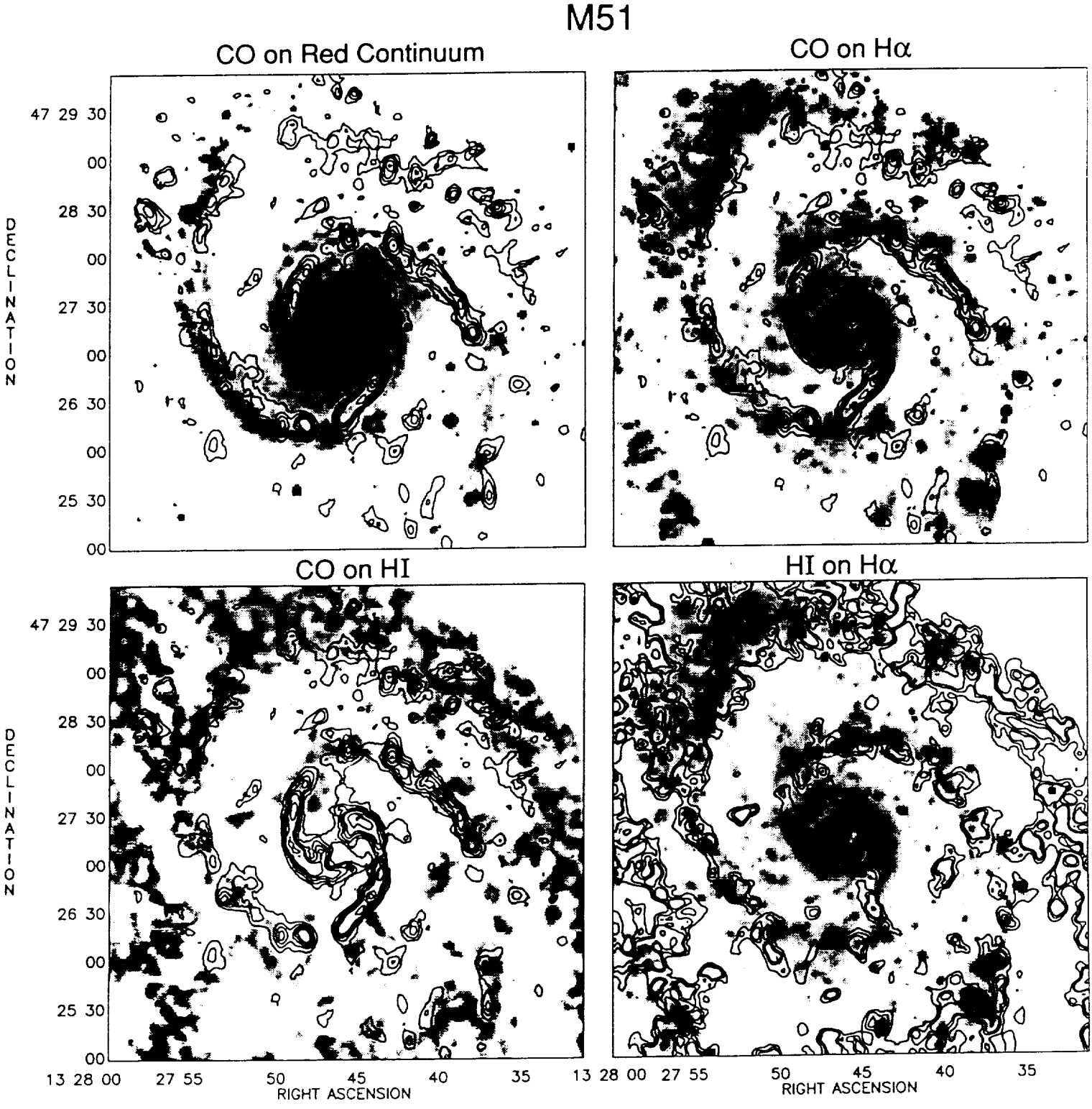
M51
CO on Red Continuum
CO on Hα
CO on HI
HI on Hα
DECLINATION
47 29 30
00
28 30
00
27 30
00
26 30
00
25 30
00
13 28 00
27 55
50
45
40
35
RIGHT ASCENSION

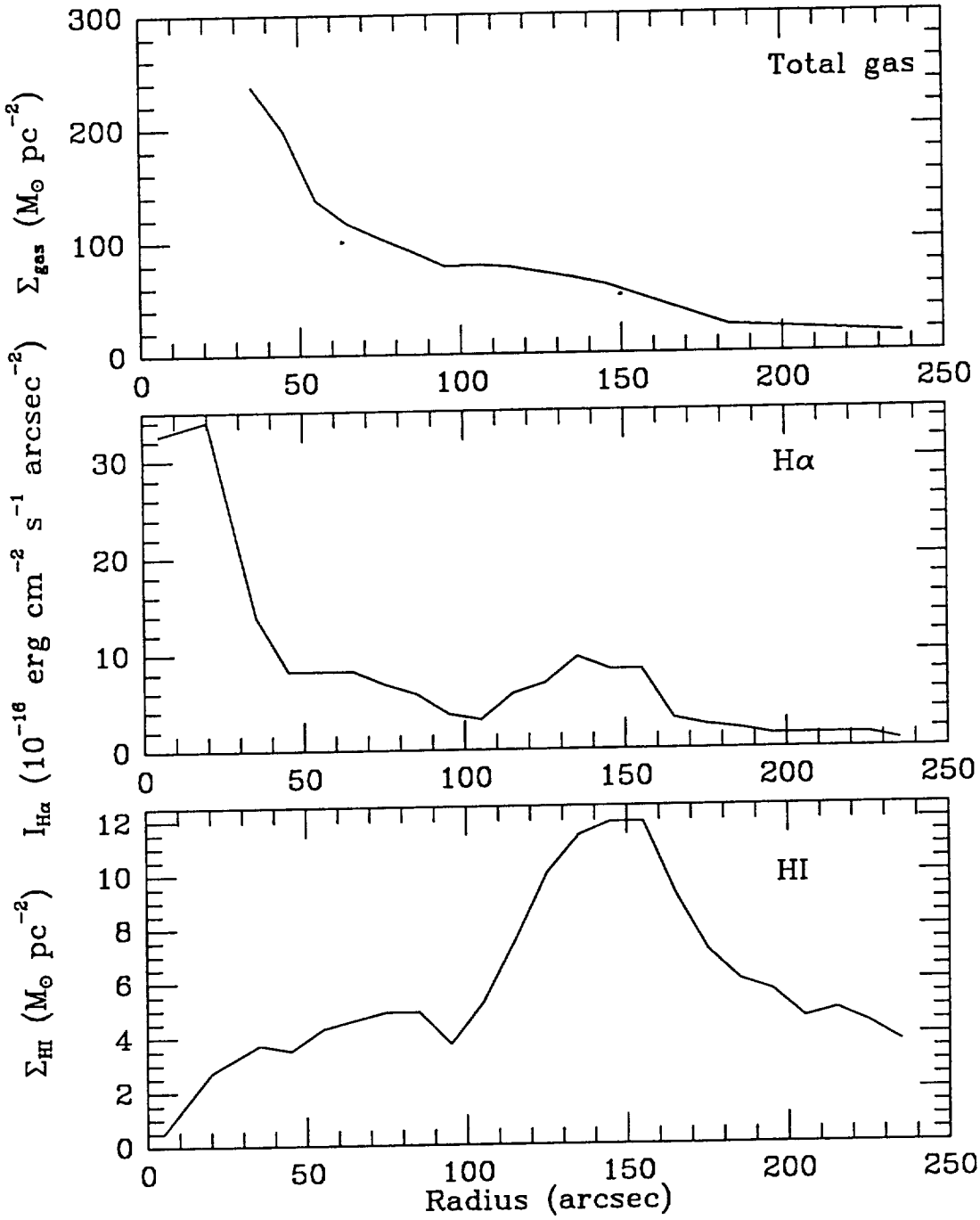
Total gas
Hα
HI
Σ_{gas} ($M_\odot$ pc^{-2})
$I_{H\alpha}$ (10^{-16} erg cm^{-2} s^{-1} arcsec^{-2})
Σ_{HI} ($M_\odot$ pc^{-2})
Radius (arcsec)
0
50
100
150
200
250
300
30
20
10
12
8
6
4
2

Fig 2

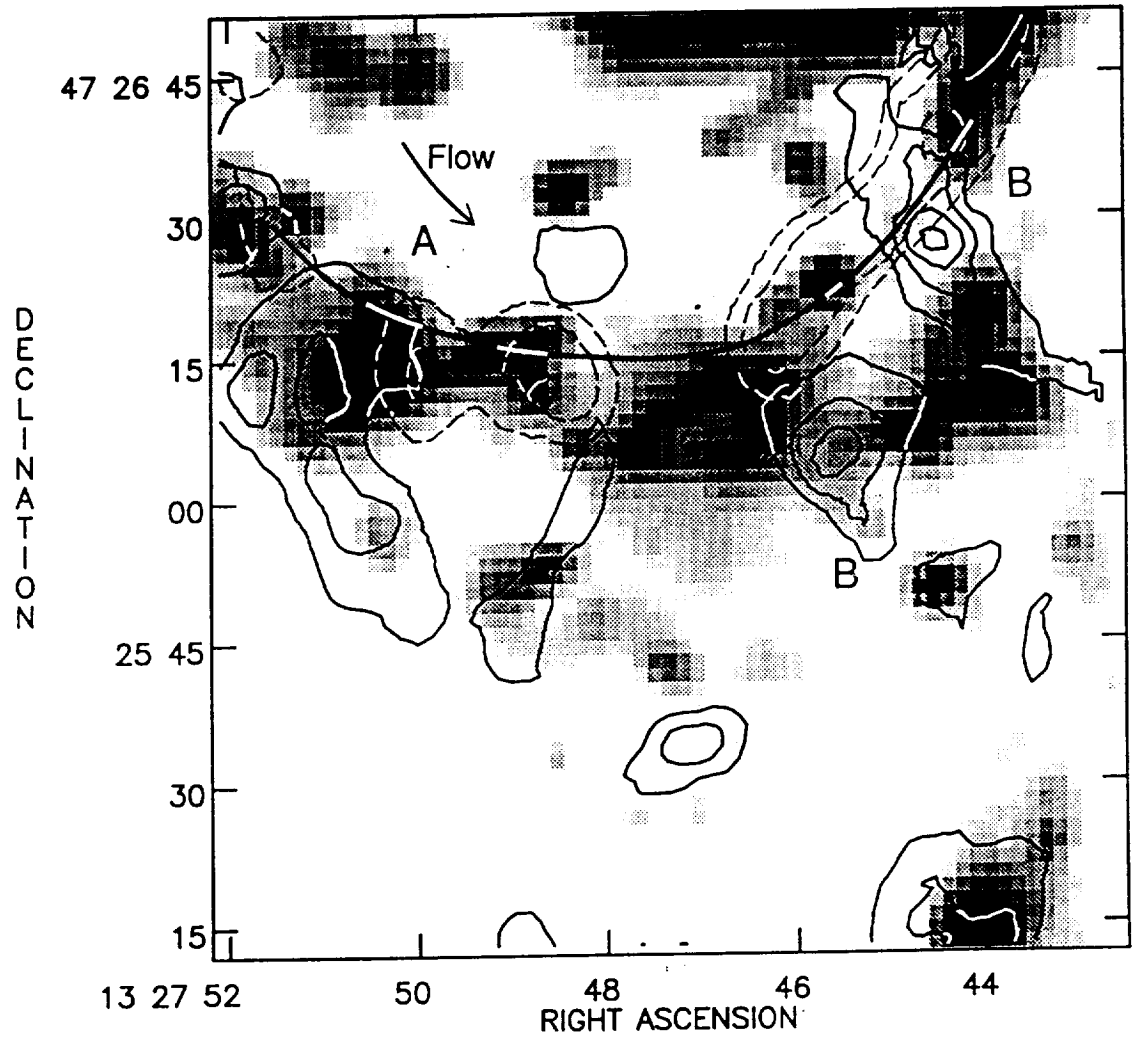
47 26 45
30
15
00
25 45
30
15
DECLINATION
Flow
A
B
B
13 27 52
50
48
46
44
RIGHT ASCENSION

Fig 4

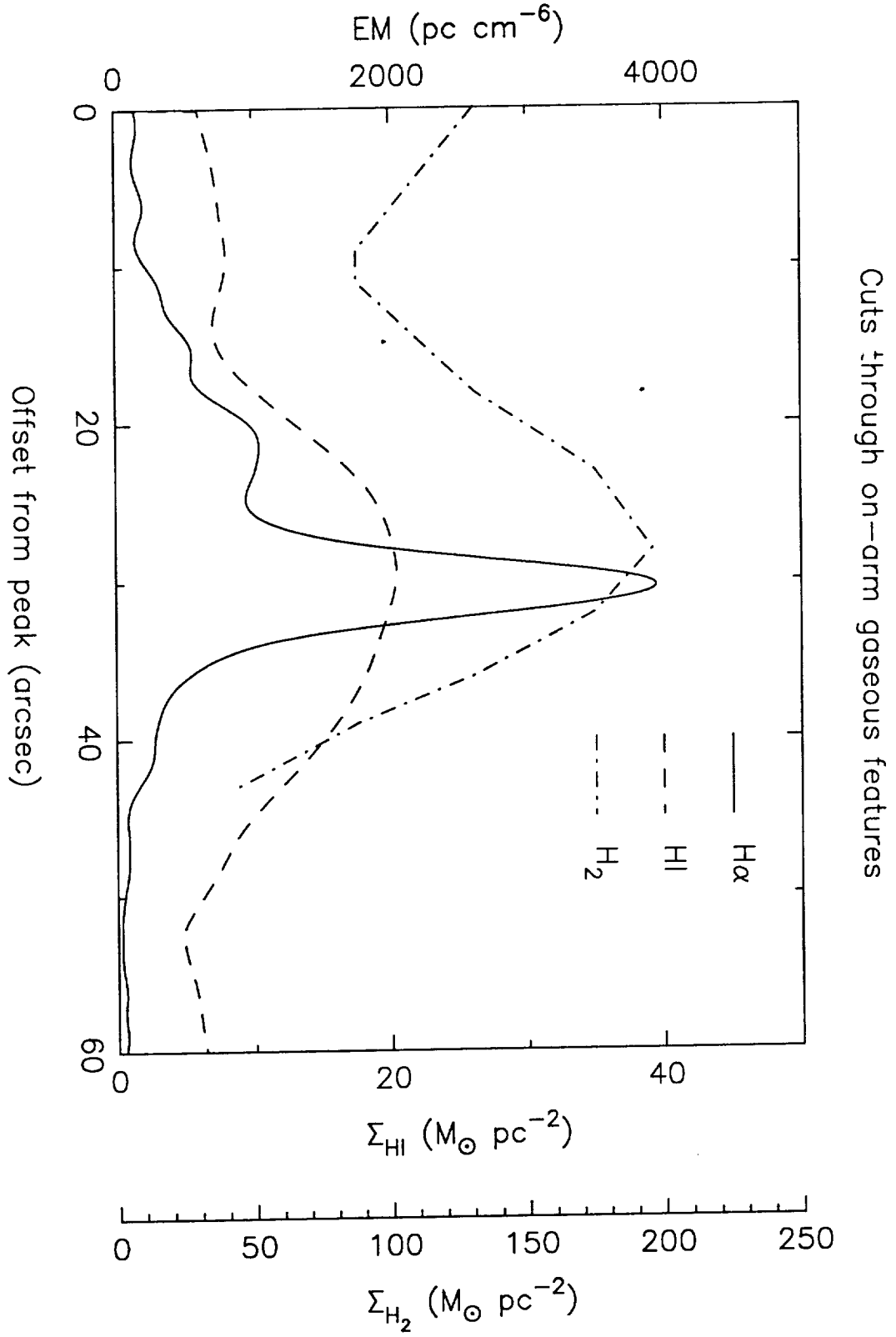
EM (pc cm^{-6})
0
2000
4000
0
20
40
60
Offset from peak (arcsec)
Hα
HI
H$_2$
0
20
40
Σ_{HI} ($M_\odot$ pc^{-2})
0
50
100
150
200
250
Σ_{H_2} ($M_\odot$ pc^{-2})
Cuts through on-arm gaseous features

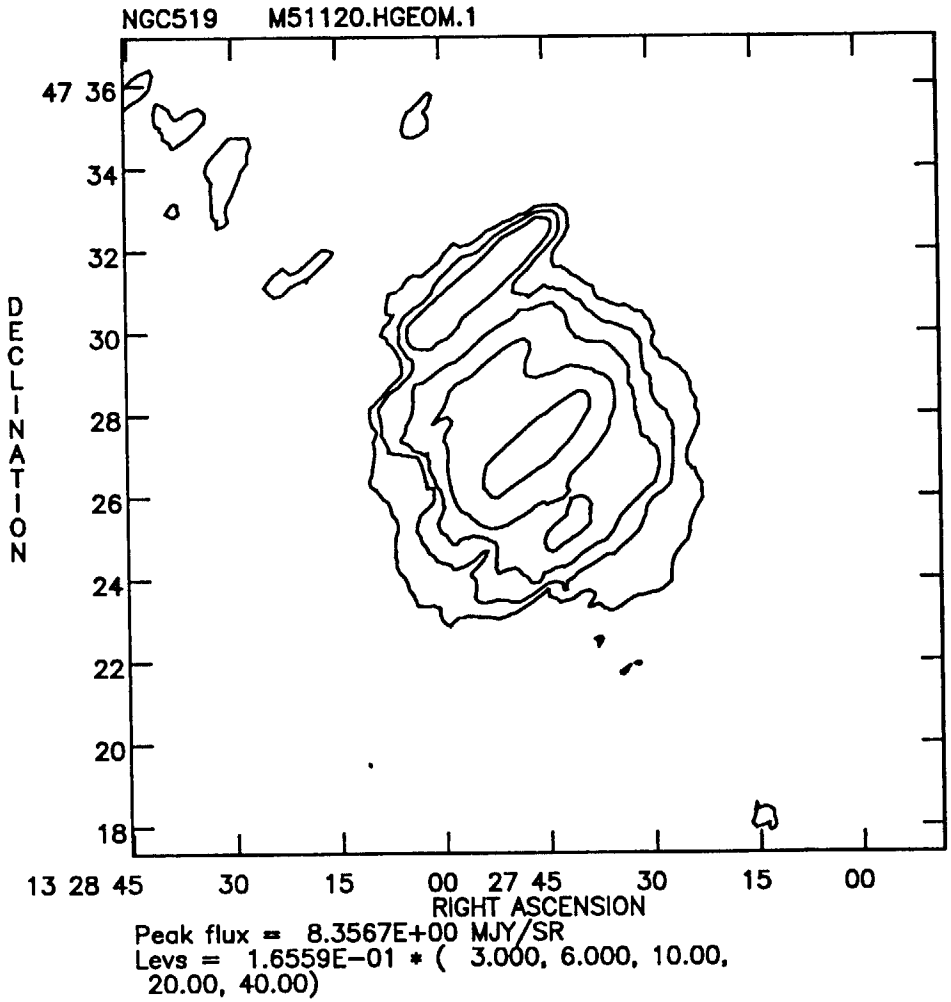
NGC519 M51120.HGEOM.1
47 36
34
32
30
28
26
24
22
20
18
DECLINATION
13 28 45
30
15
00
27 45
30
15
00
RIGHT ASCENSION
Peak flux = 8.3567E+00 MJY/SR
Levs = 1.6559E-01 * (3.000, 6.000, 10.00, 20.00, 40.00)

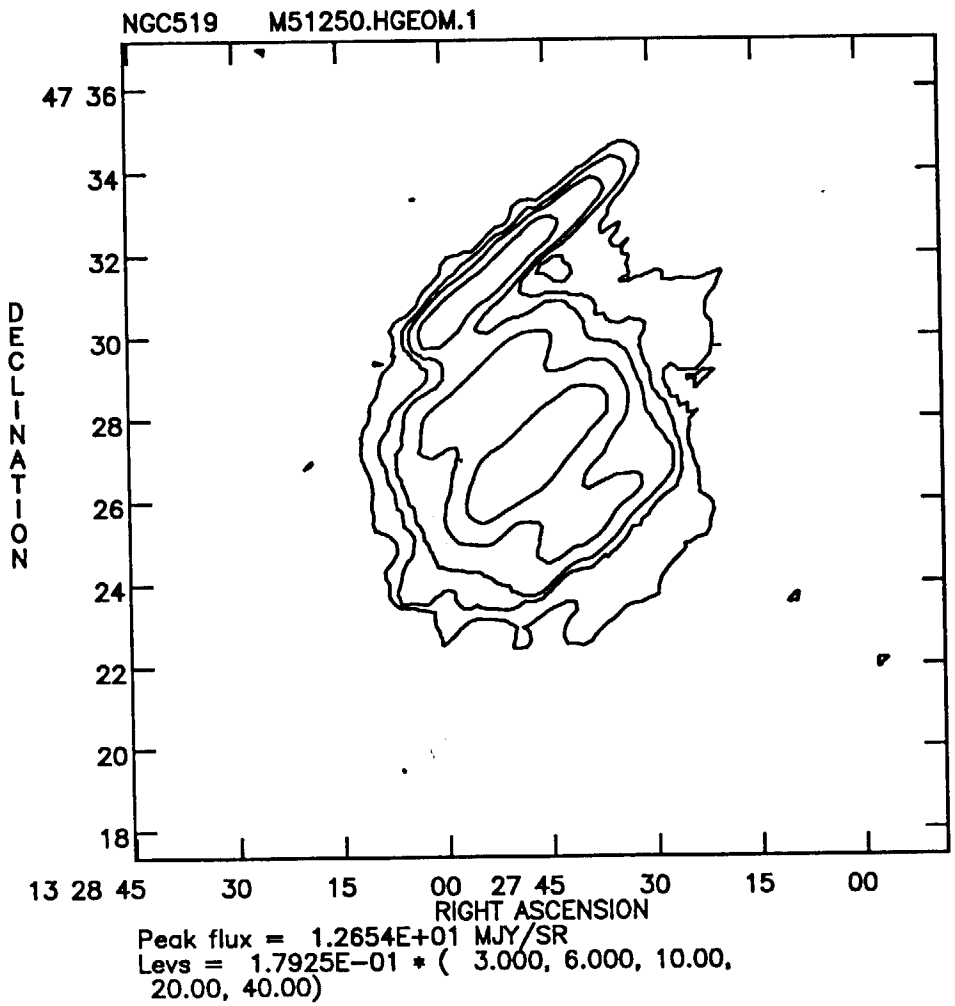
NGC519 M51250.HGEOM.1
47 36
34
32
30
28
26
24
22
20
18
DECLINATION
13 28 45
30
15
00
27 45
30
15
00
RIGHT ASCENSION
Peak flux = 1.2654E+01 MJY/SR
Levs = 1.7925E-01 * (3.000, 6.000, 10.00, 20.00, 40.00)

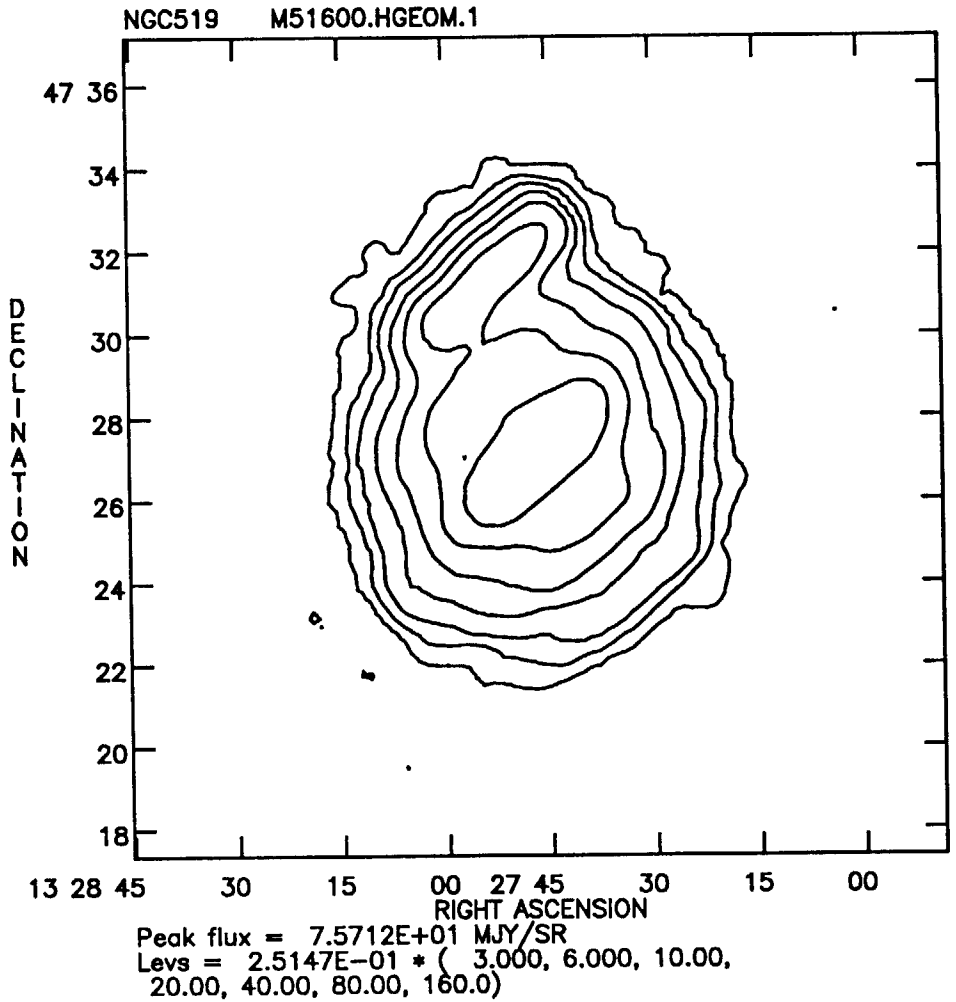
NGC519 M51600.HGEOM.1
47 36
34
32
30
28
26
24
22
20
18
DECLINATION
13 28 45
30
15
00
27 45
30
15
00
RIGHT ASCENSION
Peak flux = 7.5712E+01 MJY/SR
Levs = 2.5147E-01 * (3.000, 6.000, 10.00,
20.00, 40.00, 80.00, 160.0)

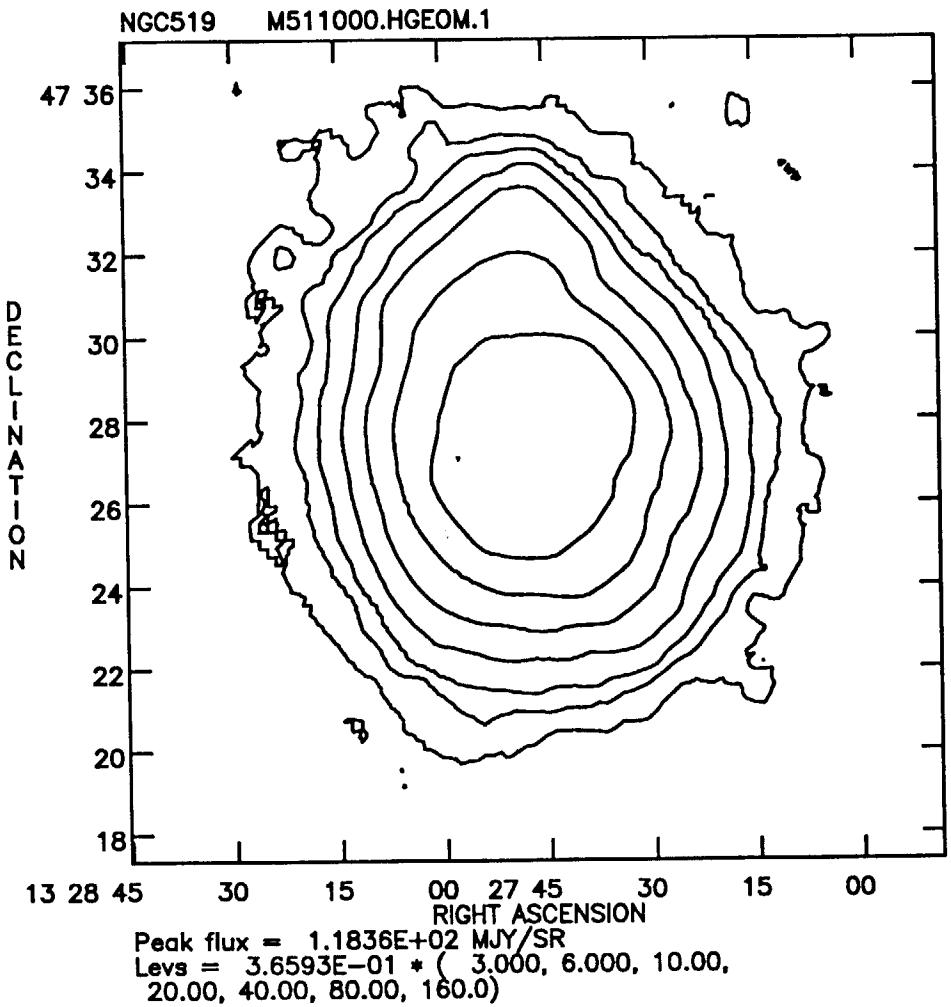

Peak flux = 1.1836E+02 MJY/SR
Levs = 3.6593E-01 * (3.000, 6.000, 10.00, 20.00, 40.00, 80.00, 160.0)

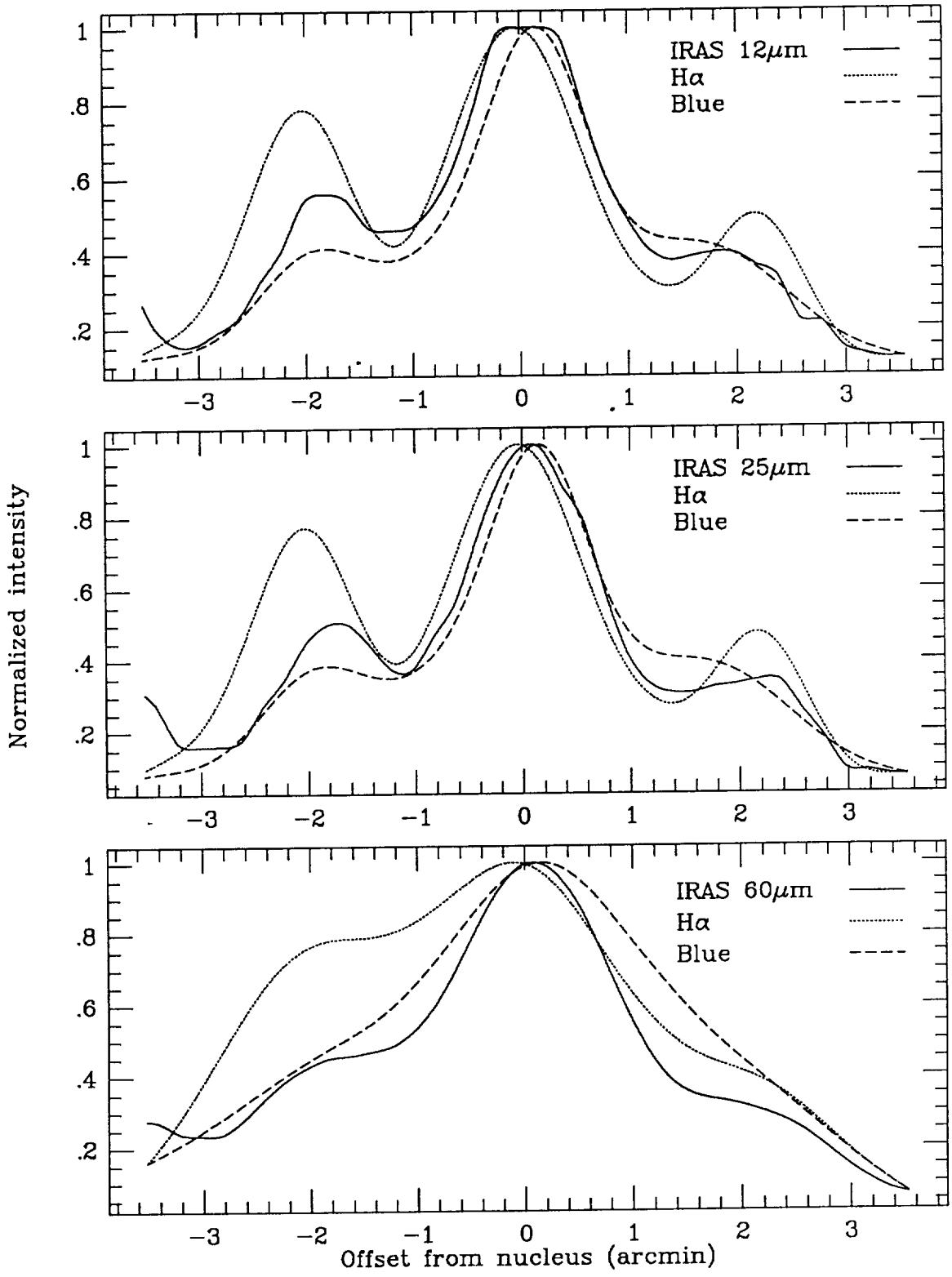
IRAS 12μm
Hα
Blue
IRAS 25μm
Hα
Blue
IRAS 60μm
Hα
Blue
Normalized intensity
Offset from nucleus (arcmin)
1
.8
.6
.4
.2
−3
−2
−1
0
1
2
3

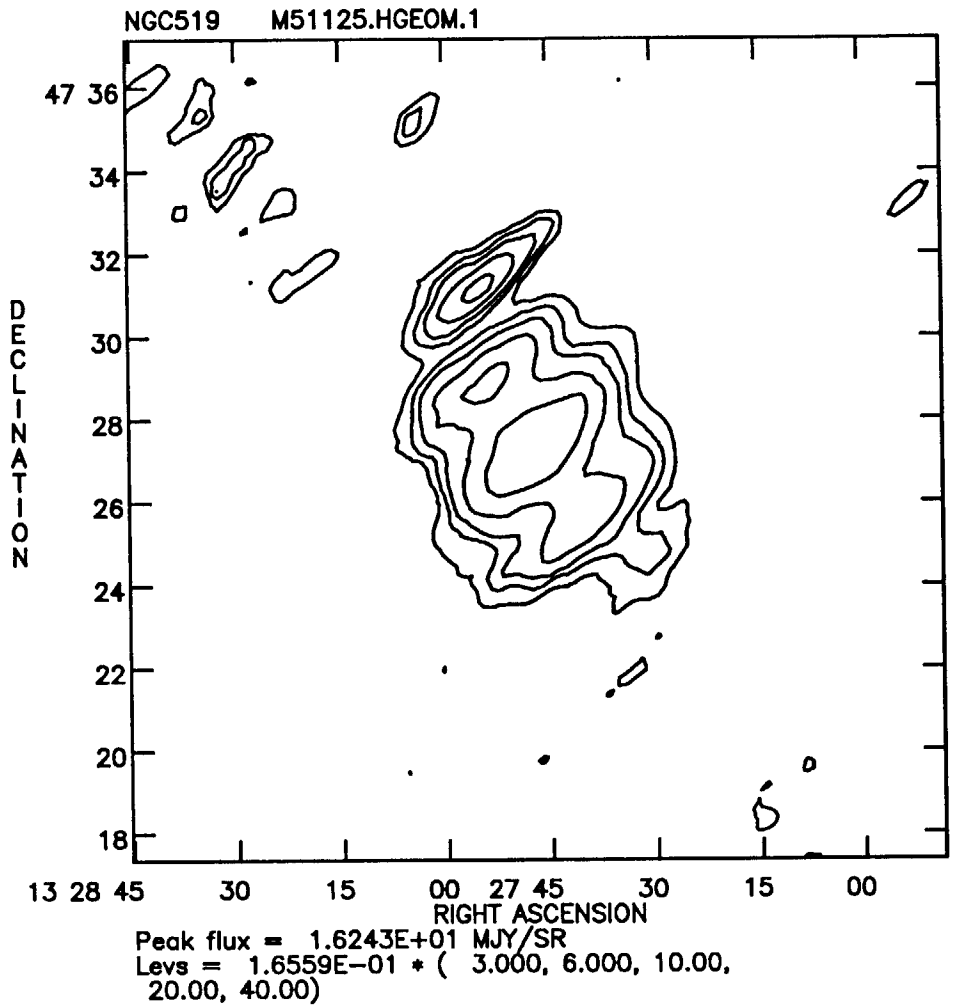
NGC519 M51125.HGEOM.1
47 36
34
32
30
28
26
24
22
20
18
DECLINATION
13 28 45
30
15
00
27 45
30
15
00
RIGHT ASCENSION
Peak flux = 1.6243E+01 MJY/SR
Levs = 1.6559E-01 * (3.000, 6.000, 10.00, 20.00, 40.00)

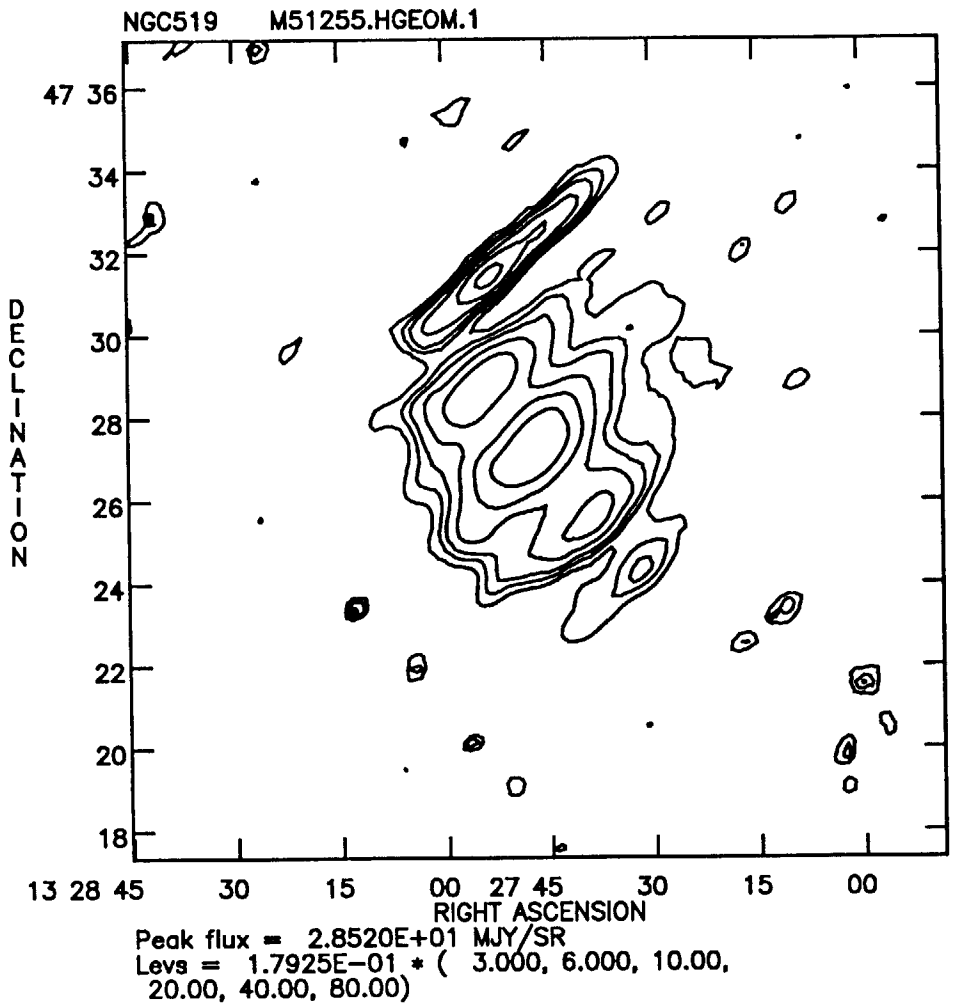
NGC519 M51255.HGEOM.1
47 36
34
32
30
28
26
24
22
20
18
DECLINATION
13 28 45
30
15
00
27 45
30
15
00
RIGHT ASCENSION
Peak flux = 2.8520E+01 MJY/SR
Levs = 1.7925E-01 * (3.000, 6.000, 10.00,
20.00, 40.00, 80.00)

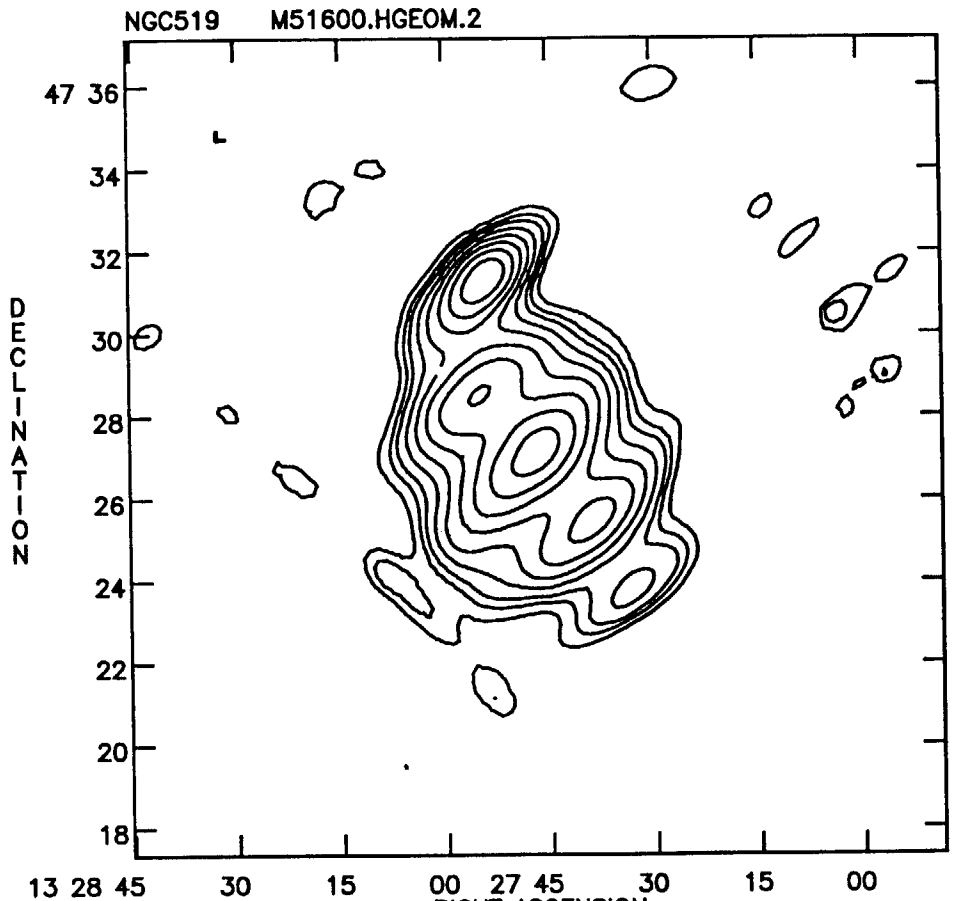

Peak flux = 2.4053E+02 MJY/SR
Levs = 2.5147E−01 * (3.000, 6.000, 10.00, 20.00, 40.00, 80.00, 160.0, 320.0, 640.0)

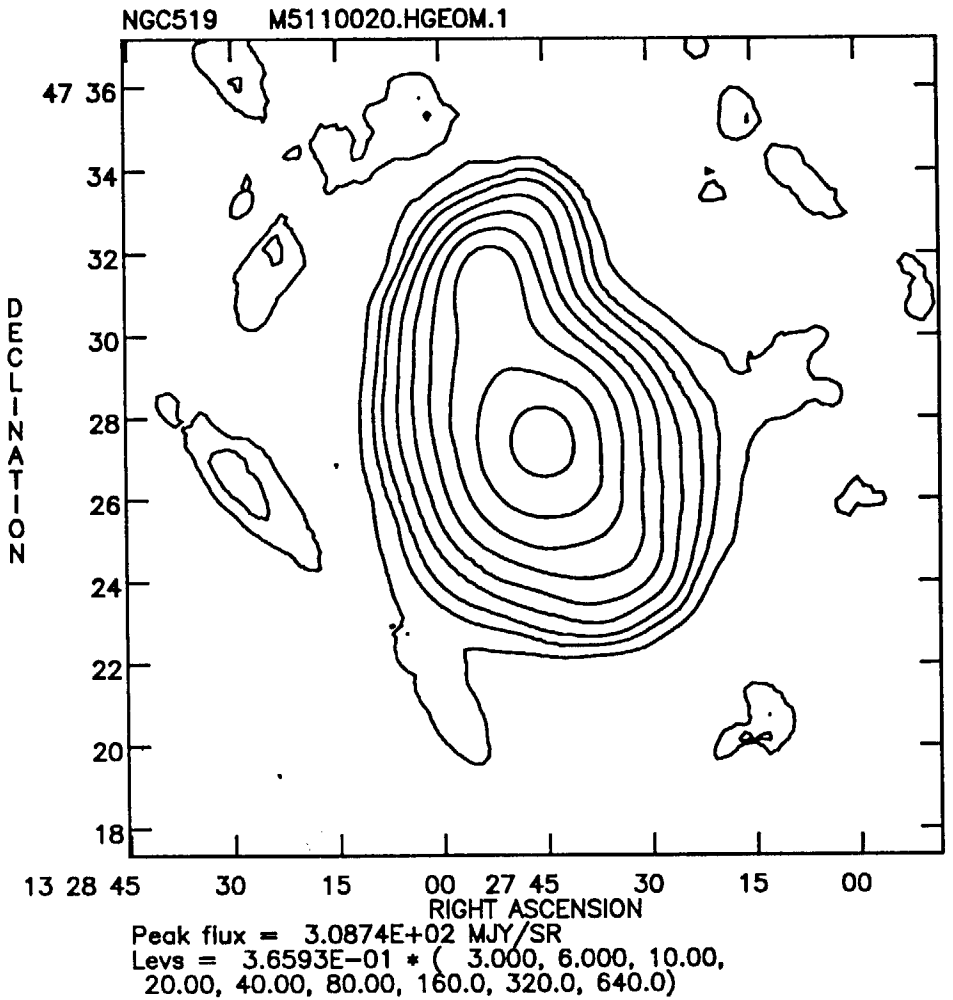
NGC519 M5110020.HGEOM.1
47 36
34
32
30
28
26
24
22
20
18
DECLINATION
13 28 45
30
15
00
27 45
30
15
00
RIGHT ASCENSION
Peak flux = 3.0874E+02 MJY/SR
Levs = 3.6593E-01 * (3.000, 6.000, 10.00,
20.00, 40.00, 80.00, 160.0, 320.0, 640.0)

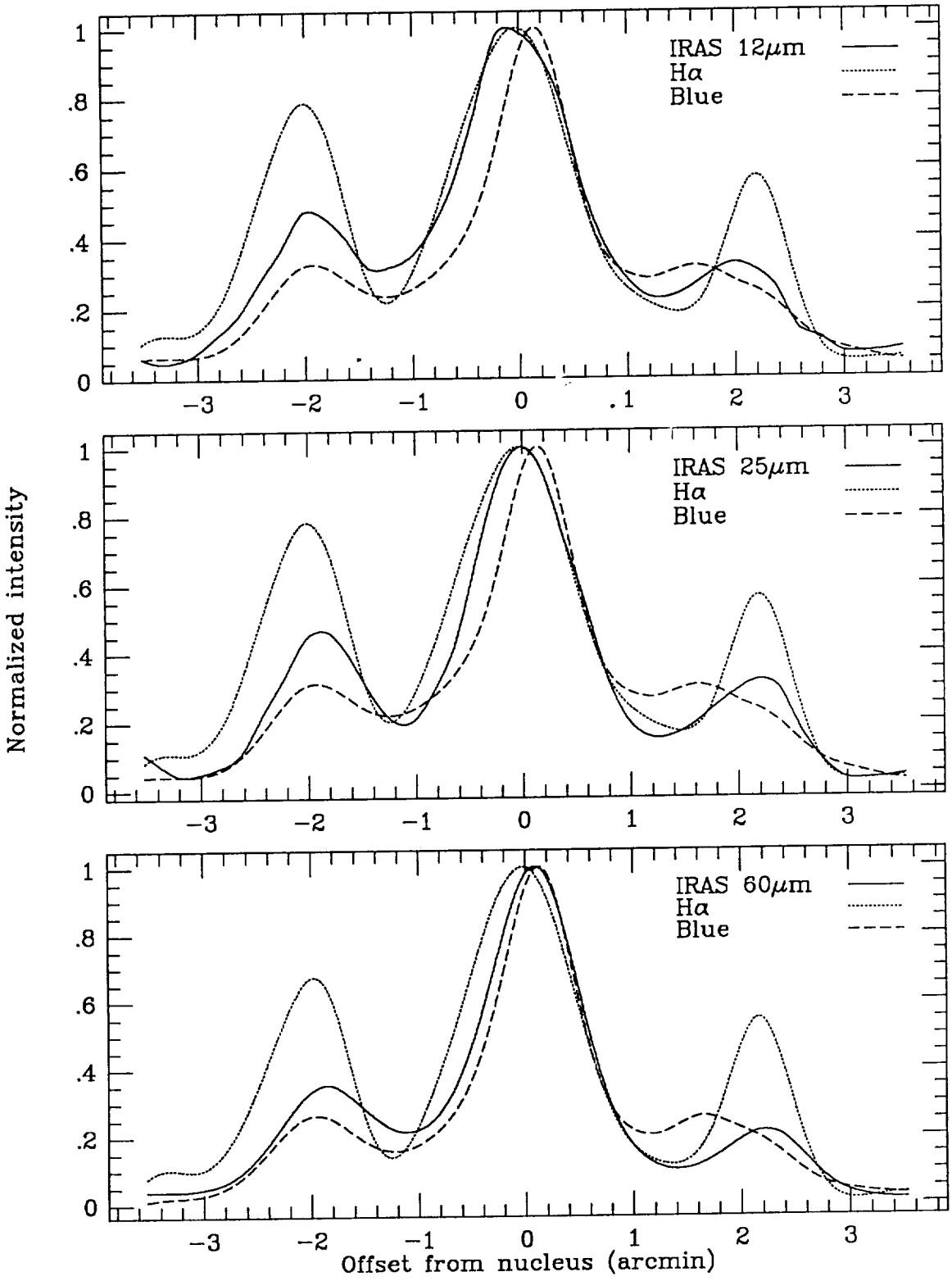
IRAS 12μm
Hα
Blue
IRAS 25μm
Hα
Blue
IRAS 60μm
Hα
Blue
Normalized intensity
Offset from nucleus (arcmin)
0
.2
.4
.6
.8
1
−3
−2
−1
0
1
2
3

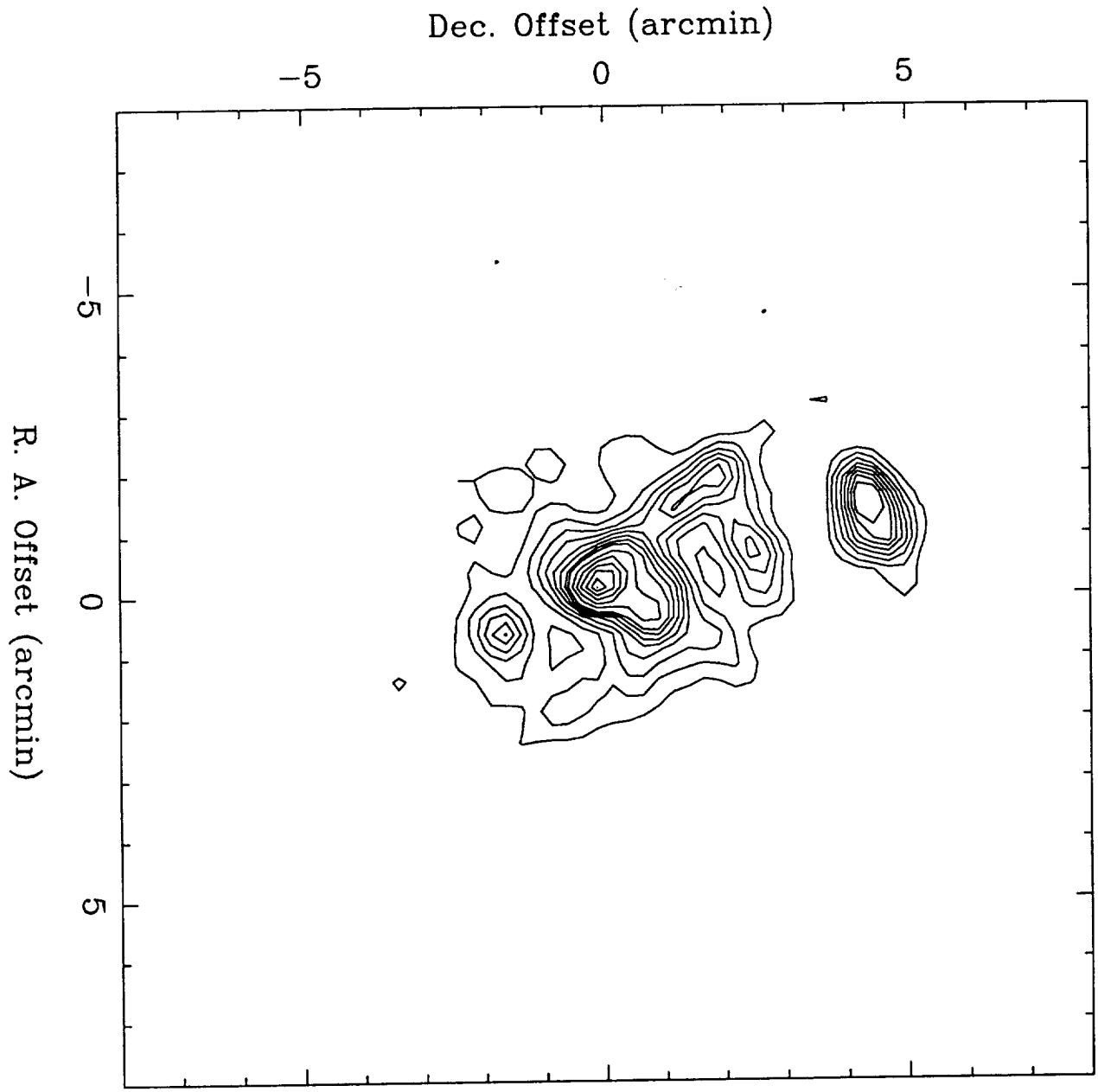
Dec. Offset (arcmin)
−5
0
5
R. A. Offset (arcmin)
−5
0
5

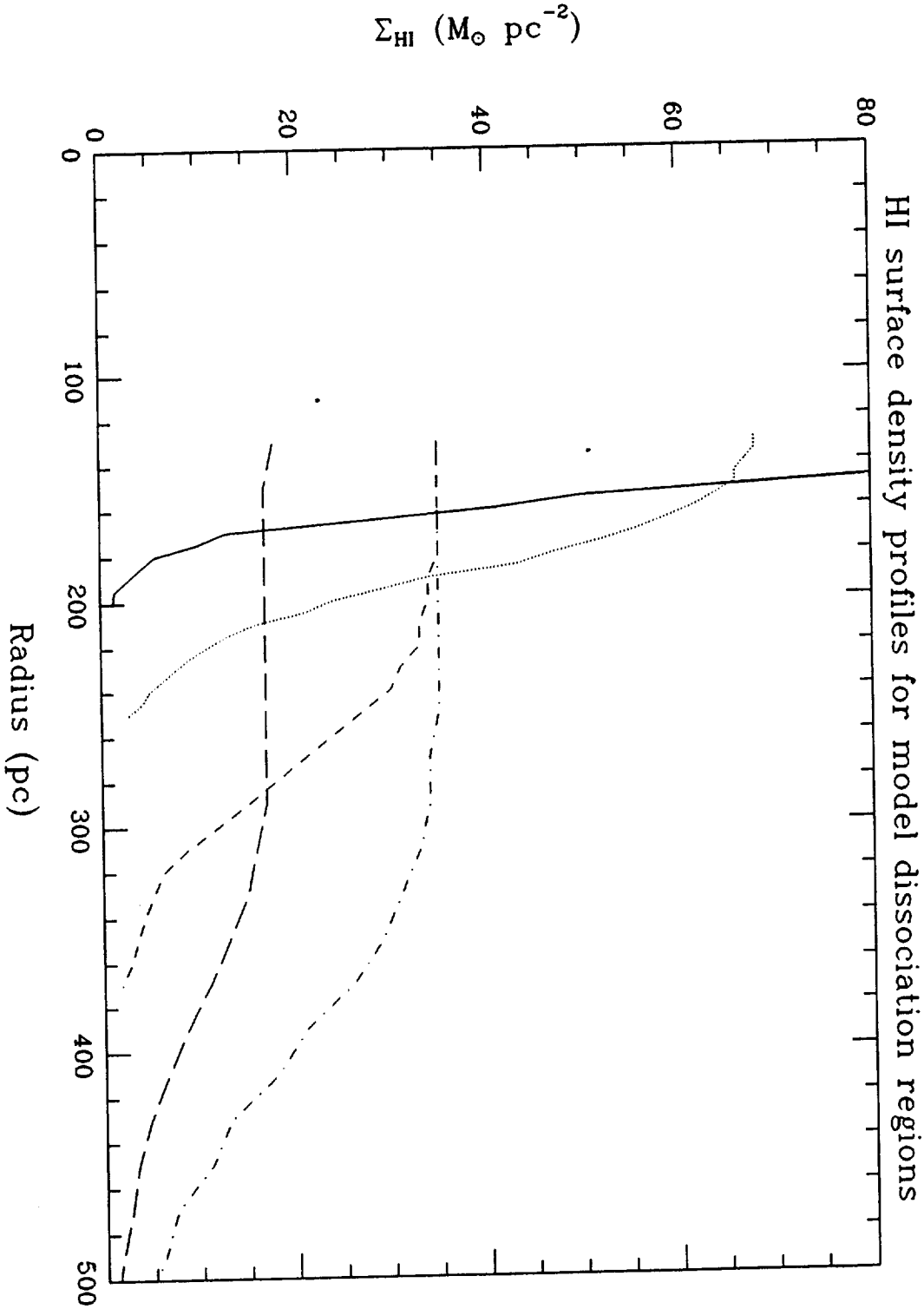
HI surface density profiles for model dissociation regions
Σ_{HI} ($M_\odot$ pc^{-2})
0
20
40
60
80
Radius (pc)
0
100
200
300
400
500